J Nanopart Res (2019) 21:249
https://doi.org/10.1007/s11051-019-4690-3

REVIEW

The role of laser ablation technique parameters in synthesis of nanoparticles from different target types

Hameed Naser · M. A. Alghoul · Mohammad Kamal Hossain · Nilofar Asim · M. F. Abdullah · Mohammed Sabah Ali · Feras G. Alzubi · N. Amin

Received: 17 May 2019 / Accepted: 15 October 2019

Abstract Optimized synthesis of nanoparticles (NPs) increased the production of ultrapure and perfectly spherical NPs with small(er) average sizes. Many methods have been reported in the literature for synthesizing NPs, with sizes of 0.01–310 nm. Laser ablation is a well-known NP preparation method. It is regarded as a physical method that needs to be carried out in a controlled setting to obtain ultrapure NPs. Most studies on laser ablation involve the preparation of many types of NPs via the utilization of multiple targets. Since laser pulse parameters, laser focusing parameters, and the medium of ablation are essential factors influencing the synthesis of NPs (size, shape, and distribution), this study comprehensively reviews their effect to classify and organize them for use by interested researchers.

Keywords Laser ablation technique · Laser pulse parameters · Laser focusing parameters · Medium of ablation ambient · Nanoparticle synthesis

Introduction

Nanoparticle synthesis routes

Nanoparticles (NPs) have seen used since the beginning of the ninth century, where artisans and craftsmen of the Mesopotamian age utilized gold and silver powders to decorate pots and utensils. This phenomenon remained a mystery up until the publication by Michael Faraday of "Experimental Relations of Gold and Other Metals to

H. Naser
Directorate of Material Research, Ministry of Science and Technology, Baghdad, Iraq

M. A. Alghoul (✉) · M. K. Hossain
Center of Research Excellence in Renewable Energy (CoRERE), Research Institute, King Fahd University of Petroleum & Minerals (KFUPM), Dhahran 31261, Saudi Arabia
e-mail: mohammad.alghoul@kfupm.edu.sa

e-mail: dr.alghoul@gmail.com

N. Asim
Solar Energy Research Institute, Universiti Kebangsaan Malaysia, 43600 Bangi, Selangor, Malaysia

M. F. Abdullah
Malaysia-Japan International Institute of Technology, Universiti Teknologi Malaysia, Jalan Sultan Yahya Petra, 54100 Kuala Lumpur, Malaysia

M. S. Ali
College of Engineering, Biomedical Engineering Department, University of Kerbala, Kerbala, Iraq

F. G. Alzubi
Energy and Building Research Center, Kuwait Institute for Scientific Research, P.O. Box (24885), 13109 Safat, Kuwait

N. Amin
Institute of Sustainable Energy, Universiti Tenaga Nasional (at The National Energy University), Jalan Ikram-Uniten, 43000 Kajang, Selangor, Malaysia

M. A. Alghoul · M. K. Hossain
Researcher at K.A.CARE Energy Research & Innovation Center at Dhahran, Dhahran, Saudi Arabia

Published online: 22 November 2019

Light" (Faraday 1857). The talk, titled "There's Plenty of Room at the Bottom" by American physicist Richard Feynman at California Institute of Technology (Caltech) on December 29, 1959, inspired and revolutionized modern nanoscience and nanotechnology (Feynman 2012; Moore et al. 2008). NPs are suitable for various applications and exhibit new and unprecedented characteristics relative to their bulk counterparts (Lindsay 2010; Moore et al. 2008). However, the synthesis of nanoscale materials requires specific and sophisticated handling, as per the route of synthesis. There are two approaches, i.e., bottom–up and top–down, shown in Fig. 1.

Pros and cons of PLA

It is well understood that amongst the available techniques for synthesizing NPs, the pulse laser ablation (PLA) route, either in liquid or solid phase, possesses several advantages over others.

In the liquid phase process, the experimental cost is minimal relative to its solid counterpart. Targets required for the synthesis are less expensive than the metal salts and other chemicals required in the chemical routes. The technique is known as a green route and for being highly reproducible. Most importantly, as-fabricated NPs are inherently surfactant-free; thus, functionalization is simple if required. The PLA technique is useful not only for synthesizing metal NPs, but it could also be used to synthesize semiconducting, magnetic and organic NPs of all shapes and sizes. However, the PLA in the liquid phase reported shortcomings such as contamination on the surface of the NPs if the process is conducted in an organic solvent medium due to the solvents pyrolyzing the organic molecules.

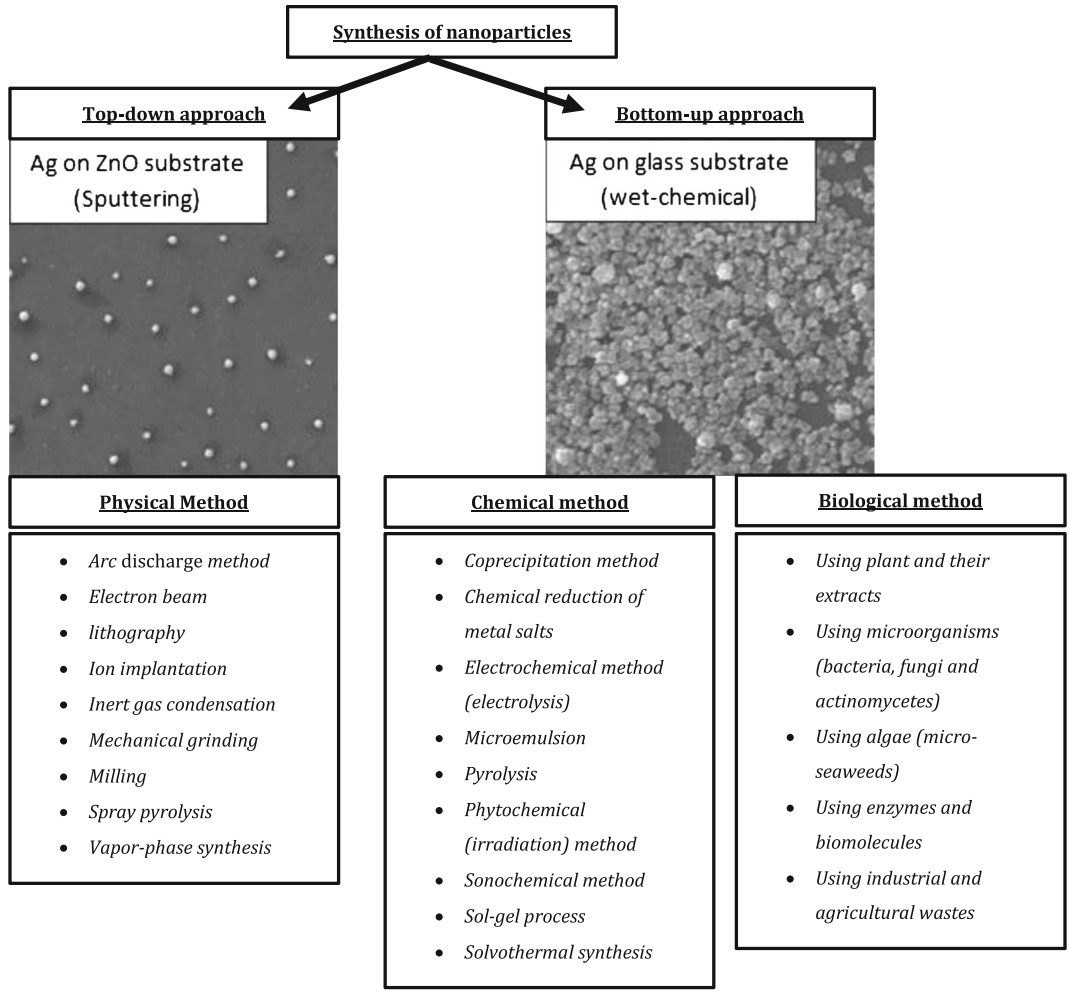

Fig. 1 Different routes to synthesis nanoparticles

Controlling the size and distribution of the as-fabricated NPs is simple but limited due to its rather simple experimental setup. As pointed out previously, the yield is reproducible, but optimizing the volume and cost remains a concern.

In the solid-phase process, most of the metals and its composites can be synthesized and deposited in various substrates. Thanks to laser technology, entire classes of lasers, encompassing continuous, pulse, short wavelength, longwave length, lower energy, and higher energy can be utilized in this process, making precise control over the deposition process possible. Since the laser is not part of the vacuum system, the process is more user-friendly and versatile vis-à-vis achieving the various types of depositions. Vacuum is an essential part of the PLA system in the solid phase as it provides a platform to deposit a thin film of various phases and structures, however, the synthesis costs increases due to the presence of chamber pressure control and the involvement of parametric optimization. There are other shortcomings related to the intrinsic nature of the ablation process and the photon (from the laser) and electron (from the target) interaction. The lack of suitable optimization often results in defects in the subsequent structures and film growth. High-intensity laser sources could incorporate microscopic and nanoscopic particles from the target, which degrades the quality of the subsequently deposited films.

Previous review work published on PLA

PLA was an invention that preceded the pulsed ruby laser in the 1960s. Many research works have subsequently explored laser ablation in vacuum/dilute gases. Many types of thin films can be synthesized by varying the target materials, background gases, and laser parameters for use in various applications, e.g., electrodes, wear-resistant coatings, and semiconductor devices (Messina 2011). The employed targets can be metals, semiconductors, oxides, high-temperature superconductors, diamond-like carbon, or (other) ceramics.

Table 1 summarizes the literature on the subject, arranged by article title, R&D aspects, and period of R&D. As apparent in Table 1, the majority of the analyzers evaluated the accepted analysis and development aspects of PLA technologies. Many researchers underlined similar R&D aspects of PLA technologies such as laser ablation inductively coupled plasma–mass spectrometry (LA-ICP-MS) (Arevalo Jr et al. 2010; Cleveland and Michel 2008; Koch and Günther 2011; Phipps et al. 2010; Russo et al. 2002; Shirk and Molian 1998; Toosi et al. 2017). There are some reviews covering certain technologies or aspects, such as laser ablation for the deposition of thin films (Auciello 1991; Gaertner and Lydtin 1994; Maier-Komor 1991), while others cover definite technologies or facets such as clinical review PLA collector (Ali et al. 2016; Chan et al. 2016; Dill et al. 2011; Zhao et al. 2017). There are also reviews on factors influencing PLA's system performance (Ahmed et al. 2016; Barefoot 2004; Cocherie and Robert 2008; Gonzalez 2017; Jackson and Palmer 1994; Kim et al. 2017; Scharring et al. 2011; Sinko and Sasoh 2011; Tsuji et al. 2012b; Yang 2007).

Many case studies are being reported on the synthesis of NPs using the laser ablation method, but there is no state-of-the-art review on factors influencing the synthesis of NPs. This study is a critical review of the factors and parameters reported in the literature on the usage of the laser ablation method. Figure 2 summarizes the factors and parameters influencing the synthesis of NPs using the laser ablation method.

Fundamentals of laser ablation technique and associated devices

Nd:YAG laser

Neodymium-doped yttrium aluminum garnet, or Nd:YAG, is a crystal used by solid-state lasers as a lasing medium . The Nd:YAG laser is optically pumped using a flash tube for laser diodes. Nd:YAG lasers emit light at a wavelength of 1064 nm (IR region).

Excimer laser ablation

An excimer laser utilizes gas as its active medium. The wavelength of the produced beam falls within 193–351 nm. The excimer laser was first reported in the late 1970s. Many improvements have been made since then on gas lifetimes, upgraded electronics for computer control, sensors for process monitoring, and scanning stage technology (Setia 2005).

Working principle of laser ablation in liquid

The apparatus required to generate PLA in the liquid is illustrated in Fig. 3. The metals were cleaned using an ultrasonic cleaner and ethanol, acetone, and deionized water afterwards to remove any remaining organic compounds. The metals were then placed inside a glass

Table 1 Summary of previous review articles in terms of the covered R&D aspects

No.	Previous review articles and covered period of study	Article title and content outlines
1	Kim et al. (2017) from 1972 to 2017.	"Synthesis of nanoparticles by laser ablation: A review": (1) Nanoparticle formation by laser ablation (basic concept of laser ablation, laser, change in the temperature by laser irradiation and nucleation and particle growth) and (2) synthesis of various kinds of nanoparticles by laser ablation (semiconductor quantum dot, metal and oxide nanoparticles and nanoparticles and nanowires).
2	Zhao et al. (2017) from 2002 to 2017.	"CT-guided percutaneous laser ablation of metastatic lung cancer: three cases report and literature review": (1) Case presentation, (2) CT-guided percutaneous laser ablation, (3) follow-up and outcome measures, (4) results, and (5) discussion.
3	Chan et al. (2016) from 1998 to 2016.	"Holmium: YAG laser ablation for the management of lower urinary tract foreign bodies following incontinence surgery: A Case Series and Systematic Review": (1) Methods (case series and systematic review); (2) results (patient demographics, operative management, patient outcomes, and systematic review); (3) discussion.
4	Ali et al. (2016) from 2001 to 2016.	"Our experience of carbon dioxide laser ablation of angiofibromas: case series and literature review": (1) Materials and methods and (2) results and discussion.
5	Ahmed et al. (2016) from 1983 to 2016.	"Laser Ablation and Laser -hybrid Ablation Processes: A Review": Laser beam machining (LBM) (physical factors affecting the process, laser radiation features, substrate material features, laser ablation mechanism, laser beam milling, ablation mechanism of laser beam milling, parametric effects in laser beam milling, laser induced periodic structures, laser beam milling with auxiliary concepts, laser beam drilling/trepanning, ablation mechanism in laser beam drilling, parametric effects in laser beam drilling, conclusions and remarks), laser-assisted machining (LAM) (material removal mechanism in LAM, parametric effects and inspirations of LAM, cutting forces and material removal rate, tool life and surface roughness, conclusions and remarks), laser chemical machining/etching (LCM/E) (LCM/E mechanism, parametric effects and inspirations of LCM/E, porous structures, 3D structures, conclusions and remarks), laser-assisted electrochemical machining (LAECM), (conclusions and remarks), underwater laser ablation (UWLA) (UWLA mechanism, water layer thickness, splashing and cavitation bubbles, melt ejection and sample configuration, parametric effects of UWLA, high ablation rate, low ablation rate, possible reasons of ablation rate variations, Inspirations of UWLA, under water laser milling, under water laser drilling, synthesis of nanoparticles, conclusions and remarks), shortfalls, and areas of future research.
6	Scharring et al. (2011) from 1988 to 2011.	"Review on Japanese-German-U.S. Cooperation on Laser-Ablation Propulsion": Methods (experimental setup, laboratory setup Nagoya, laboratory setup Stuttgart, result, and discussion),

Table 1 (continued)

No.	Previous review articles and covered period of study	Article title and content outlines
		beam propagation modeling and profilometry of ablative targets (Nagoya–Stuttgart), impulse coupling of flat POM targets in ambient air (Nagoya–Stuttgart), nozzles and flat targets in ambient air (Nagoya–Stuttgart), nozzles and flat targets in vacuum (Nagoya).
7	Sinko and Sasoh (2011) from 1972 to 2011.	"Review of CO2 Laser Ablation Propulsion with Polyoxymethylene": (1) Material characteristics (chemical formula and basic properties, thermal properties, thermal degradation, reflectivity and transmissivity, absorption coefficient (mass removal and impulse models, photochemical mass removal, photothermal mass removal, comparing photochemical and photothermal pathways)), (2) experimental environment (CO_2 lasers, ambient condition, conditioning effects), (3) measurement techniques (ablated mass, imparted impulse, laser pulse energy, laser spot area), (4) impulse performance (fluence-dependent, impulse modeling in vacuum, ambient pressure dependence, spot area dependence, combustion and confinement effects, doping and other effects), (5) conclusions and recommended works
8	Koch and Günther (2011) from 1985 to 2011.	"Review of the State-of-the- Art of Laser Ablation Inductively Coupled Plasma Mass Spectrometry": Fundamentals (laser–material interaction, aerosol formation and transportation), inductively coupled plasma mass spectrometry system configuration (mass analyzers and mass spectrometry detection schemes, inductively coupled plasma operating conditions), data processing and analysis (elemental fractionation, matrix-matched calibration: nanosecond versus femtosecond LA-ICP-Q-MS, in-depth and layer analysis by fs-LA-ICP-Q MS).
9	Dill et al. (2011) from 1985 to 2011.	"Dating of Pleistocene uranyl phosphates in the supergene alteration zone of Late Variscan granites by Laser-Ablation-Inductive-Coupled-Plasma Mass Spectrometry with a review of U minerals of geochronological relevance to Quaternary geology": (1) Laboratory methods, (2) geological and geomorphological setting, (3) results (petrography of host rock and mineralogy of supergene minerals, dating of supergene uranium minerals LA-ICP-MS), (4) discussion—age of uranyl phosphates and weathering pits.
10	Arevalo Jr et al. (2010) from 2008 to 2010.	"GGR Biennial Review: Advances in Laser Ablation and Solution ICP-MS from 2008 to 2009 with Particular Emphasis on Sensitivity Enhancements, Mitigation of Fractionation Effects and Exploration of New Applications": Enhanced sensitivity and reduced elemental/isotopic fractionation during LA-ICP-MS (femtosecond laser ablation, modified LA-ICP-MS engineering), internal standard and matrix independent measurements of major, minor and trace elements (LA-ICP-MS, solution ICP-MS), material forensic ICP-MS

Table 1 (continued)

No.	Previous review articles and covered period of study	Article title and content outlines
		applications: criminal and nuclear (markers of human provenance, Nuclear forensic materials), high-precision elemental and isotopic measurements via LA-ICP-MS ((ultra)trace element determinations, high-precision isotopic determinations).
11	Phipps et al. (2010) from 1975 to 2010.	"A Review of Laser Ablation Propulsion": What laser ablation propulsion offers, (how these benefits are achieved), early historical background, theory (plasma regime, polymers in the vapor regime, elemental materials in the vapor regime, combined models), applications (flights in air, space engines), propellants, advanced concepts (kw liquid-fueled laser-plasma engine) orion (laser launch into low earth orbit (leo)), promise for the future (1 to 2 years, 2 to 10 years, 5 to 10 years).
12	Gonzalez (2017) from 1997 to 2017.	"Laser Ablation–Based Chemical Analysis Techniques: A Short Review": Classification and discrimination analysis (bulk analysis), spatially resolved chemical analysis: chemical mapping and depth profiling (chemical mapping, depth profiling), laser ablation as a sampling tool for optical spectroscopy and mass spectrometry (LA-ICP-OES, LA-ICP-MS, LIBS, LAMIS).
13	Toosi et al. (2017) from 1989 to 2017.	"Fabrication of Micro/Nano Patterns on Polymeric Substrates Using Laser Ablation Methods to Control Wettability Behaviour: A Critical Review": (1) Wetting states, regimes, and roughness (contact angle, contact angle hysteresis), (2) laser ablation: experimental setup, (3) laser ablation of polymeric surfaces (polytetrafluoroethylene (PTFE), polylactide (PLA and PLLA), poly(methyl methacrylate) (PMMA), polydimethylsiloxane) (PDMS)).
14	Tsuji et al. (2012b) from 1993 to 2012.	"Preparation and Shape-Modification of Silver Colloids by Laser Ablation in Liquids: A Brief Review": (1) Methodology, (2) preparation of silver NPS using LAL in PVP solution (influence of PVP on the stability of colloids, influence of PVP on the particle size, influence of PVP on the formation efficiency, time-resolved imaging of the LAL process), (3) shape modification of silver NPs using PLI (fragmentation of NPs, formation of nanocrystals).
15	Cocherie and Robert (2008) from 1993 to 2008.	"Laser ablation coupled with ICP-MS applied to U–Pb zircon geochronology: A review of recent advances": (1) Review of instrumentation and operating conditions (the laser, ICP-MS, blank, and common-Pb correction), (2) proposed strategy (instrumentation and operating conditions), (3) LA-MC-ICPMS results compared to TIMS and SHRIMP (zircon from Cinque Frati quartz–syenite (Corsica), zircon from tanzania (1419), zircon from Canada (UQ-Z1), zircon from Antarctica (PMA-7)).
16	Cleveland and Michel (2008) from 1996 to 2008.	"A Review of Near-Field Laser Ablation for High-Resolution Nanoscale Surface Analysis": Introduction to the near-field optical region (near-field laser ablation solid sampling, near-field laser

Table 1 (continued)

No.	Previous review articles and covered period of study	Article title and content outlines
		ablation solid sampling), application of the near-field effect to nanoscale laser ablation solid sampling (near-field laser ablation solid sampling, probe methods of near-field laser ablation, near-field laser ablation solid sampling, near-field laser ablation solid sampling, near-field laser ablation solid sampling, probeless methods of near-field laser ablation with nanoparticles).
17	Yang (2007) from 1976 to 2007.	"Laser ablation in liquids: Applications in the synthesis of nanocrystals": (1) Laser ablation of solids in gas environments, (2) laser ablation of solids in liquid environments (fundamental aspects, applications), (3) physical and chemical aspects of nanocrystal formation in laser ablation of solids in liquids (nucleation thermodynamics, phase transition, kinetic growth), (4) applications in synthesis of nanocrystal (diamond and related nanocrystals, metal, alloying, oxide, and other nanocrystals).
18	Barefoot (2004) from 1998 to 2004.	"Determination of platinum group elements and gold in geological materials: a review of recent magnetic sector and laser ablation applications": (1) SF-ICP-MS (introduction, applications), (2) laser ablation sampling for inductively coupled plasma mass spectrometry (LA-ICP-MS) (introduction, applications).
19	Russo et al. (2002) from 1982 to 2002.	"Laser ablation in analytical chemistry—a review": (1) Experimental systems (lasers for ablation, ablation stage, detection systems, sample preparation), (2) calibration strategies in LA-ICP-MS and LA-ICP-AES (matrix-matched direct solid ablation, dual introduction (sample-standard), direct liquid ablation), (3) elemental fractionation during laser ablation sampling (intrinsic fractionation, crater influence, transport process, fractionation and matrix effects in the ICP), (4) gas effects, (5) applications (environmental applications, geological application, archaeology applications, waste-sample analysis, other applications).
20	Shirk and Molian (1998) from 1985 to 1998.	"A review of ultrashort pulsed laser ablation of materials": (1) Types and capabilities of ultrashort pulsed lasers (dispersion induced by optical materials, gain narrowing), (2) the state of the art of ultrashort pulsed laser materials processing (metals, polymers, ceramics), (3) laser-material interactions (photon absorption processes, thermal conduction in solids, material removal mechanisms and models).
21	Jackson and Palmer (1994) from 1965 to 1994.	"Oxide superconductor and magnetic metal thin film deposition by pulsed laser ablation: a review": (1) Experimental arrangement, (2) the ablation process (the laser-target interaction, the plume of ablated material), (3) controlling film growth (choice of background pressure, substrate temperature, laser power density effects, film uniformity, droplets on the film surface, pulse repetition rate, rate control), (4) other materials prepared by laser ablation deposition (magneto-optic recording media, piezoelectric ceramics, titanium nitride, iron), (5) comparison of laser ablation with vacuum

Table 1 (continued)

No.	Previous review articles and covered period of study	Article title and content outlines
		evaporation and sputtering as methods of growing thin films (vacuum evaporation, sputtering, laser ablation deposition).
22	Gaertner and Lydtin (1994) from 1974 to 1994.	"Review of ultrafine particle generation by laser ablation from solid targets in gas flows": (1) Review and status of laser generation methods, (2) features of UFP generation by laser ablation (characterization, controlling UFP -size: mean size, size distribution, aggregates and agglomerates, generation rate dependence on material and scaling with mean laser power; hot or cold ablation, collection methods).
23	Maier-Komor (1991) from 1972 to 1991.	"A review of laser ablation techniques for the preparation of vacuum deposited isotope targets": (1) Choice of the laser for isotope target preparation, (2) experimental arrangements, (3) preparation of isotope targets (laser ablation with the CW beam, laser ablation with the long pulse laser beam, laser ablation with high power density laser pulses of < 10 ns duration).
24	Auciello (1991) from 1966 to 1991.	"A critical review of laser ablation-synthesis of high temperature superconducting films": (1) Analysis of basic phenomena (laser-induced compositional and topographical changes on target surfaces, characterization of the laser ablated-target species plume and its relation to the composition and structure of the deposited films), (2) film processing to achieve the high temperature superconducting state.

beaker containing a small volume of millimole liquid that is a millimeter above the target. The beaker was fixed on a turntable to prevent it from damaging the generated laser beam. An Nd:YAG laser irradiates the target a few pulse repetition rates, with each pulse lasting a few ns. The laser is focused using a lens with a focal length and target position of a few millimeters. The laser ablation process utilizes wavelengths of (355, 532, and 1064 nm).

Working principle of laser ablation in gas

Synthesizing NPs using the pulsed laser ablation deposition (PLAD) method is detailed in Fig. 4. A stainless-steel vacuum chamber (multi-view ports) is used at room temperature for the ablation and deposition of the material. The vacuum is created using a mix of rotary and turbo molecular pumps operating at base pressure. The target rod can rotate and moves linearly along the axis of the chamber.

Laser ablation is known to degrade surfaces. This effect, however, can be corralled by making provisions for the movement of the target rods. An Nd:YAG laser (Continuum Surelite) is used in this process at wavelengths of 1064, 532, and 355 nm. Each pulse lasts for a few nanoseconds, and a few pulses are sent every second, which creates a bright plume of plasma perpendicular to the target that permeates in all directions into the gas medium. This plume consists of high-temperature species of ions, electrons, atoms, and a cluster of a few atoms. Optics collects and focuses the resultant light to the entrance of a spectrometer.

An intensified CCD camera records the output of the spectrometer, which is then analyzed using specialized computer software.

Effect of laser pulse parameters on nanoparticles preparation

Effect of laser pulse wavelength

The distinctive absorption of the target material at specific wavelengths results in varying concentrations, which influences the particle sizes. However, it should also be

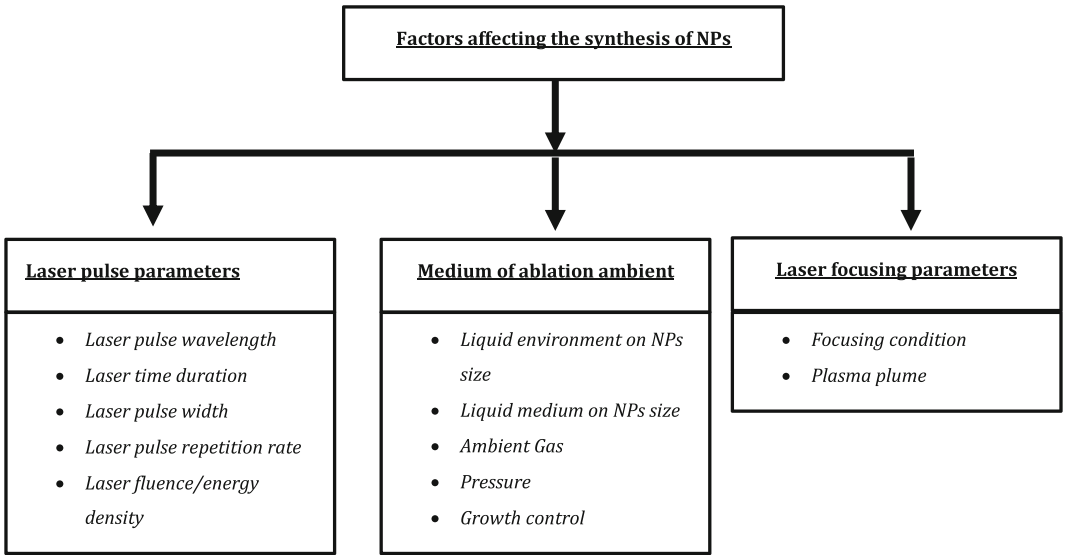

Fig. 2 Factors and associated parameters affecting the synthesis and production of NPs using laser ablation method

pointed out that the morphology of the resulting materials remains unaffected (Chewchinda et al. 2013). Smaller particle sizes result in thermal fluctuations and instability within the shape (Swarnkar et al. 2011). Interest in NPs is currently increasing due to the ubiquity of miniature electronics requiring enhanced material characteristics. Therefore, size control is crucial due to the dependence of the materials' physico-chemical properties on its size. Metal colloids report excellent optical properties and catalytic activity, making it a critical nanomaterial. Laser ablation in a solution represents a viable option for the synthesis of metal colloids. This method does not require chemical reagents to synthesize pure colloids. It has been reported that irradiating laser pulses at 1064 nm decreases the size of Ag colloids due to the self-absorption of laser pulses by the colloidal particles within the solution (Solati et al. 2013). It has also been shown that increasingly radiating colloidal solution post-ablation will result in smaller particles (Tsuji et al. 2008), which was also seen in the case of Au colloids prepared using a 1064-nm laser, with additional irradiation at 532 nm. These values proved that it is indeed possible to control the size of the colloids by altering the total number of laser pulses. The size can also be altered by changing the photon energy of laser (wavelength), but it should also be pointed out that increased wavelength will result in increased

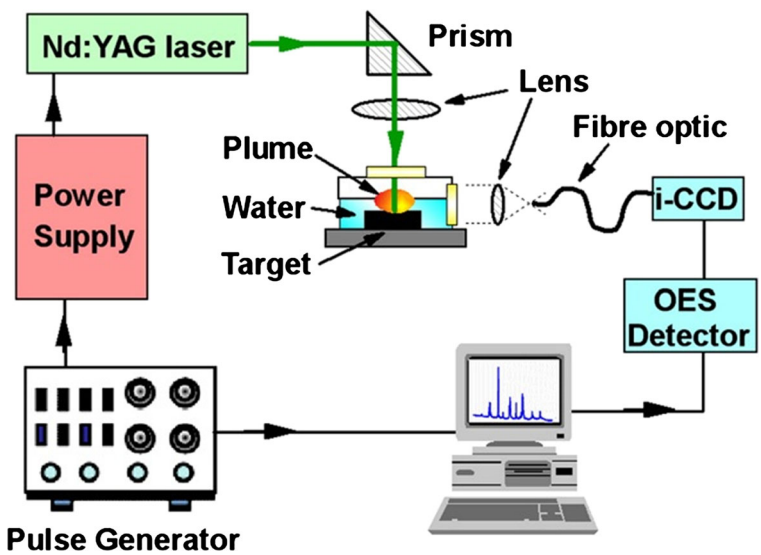

Fig. 3 Schematic diagram of the experimental setup for pulsed laser ablation in liquid (Yang et al. 2007)

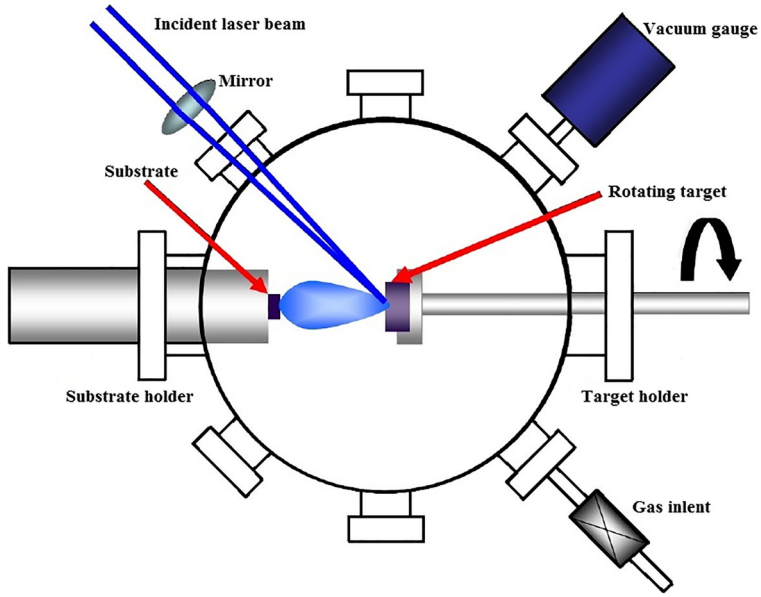

Fig. 4 Schematic of experimental setup for pulsed laser ablation in gas (Wang 2013)

particle sizes (Patra et al. 2016). Table 2 summarizes the reported works in the literature on the impact of laser wavelength and laser fluence on the synthesized NPs for different targets at different work conditions.

Effect of variation of laser time duration

The UV–visible absorption characteristics of the synthesized NPs' sizes are strongly correlated to the laser ablation time (LAT) and laser fluence (LF). The influence of the parameters on the size of the NPs was elucidated using a collection of experiments. Increased ablation time led to both increased NP density and decreased liquid molecules (Chaturvedi et al. 2017).

An example of this is the synthesis of Cu NPs, where LAT was varied from ~ 10 to 50 min, rendering the LF fixed at 151 J/cm^2 (Desarkar et al. 2012b).

The Mie theory was utilized to examine the results, culminating in the extraction of the scattering parameter and bulk copper damping frequency. It was found that surface plasmon resonance (SPR) line width is inversely proportional to the particle size, due to the intrinsic size effects. Figure 5 a and b display the variations of the SPR wavelengths and

Table 2 R&D on the effect of laser wavelength and laser fluence on the produced NPs

Author	Fluid	Wavelength (λ)	Target	Fluence	Particle size
Torrisi and Torrisi (2018)	Deionized water	355, 532, and 1064 nm	Au	10–50 J/cm^2	The average size of 10, 20, and 25 nm
Solati et al. (2013)	Acetone	1064 nm and 532 nm	Silver	14–22 J/cm^2	12.99 to 186.46 nm
Chewchinda et al. (2013)	Ethanol	1064 and 532 nm	Si	1.2 J/cm^2	3.01 to 6.98 nm
Solati et al. (2018)	Liquid nitrogen	1064–532 nm	Graphene	0.5–0.8 J/cm^2	The average size of 60.68–34.19 nm
Singh et al. (2017a)	Deionized water	1062 nm	Ti	85 W	The diameter of the 3–32 nm
Kim et al. (2014)	Deionized water	355, 532, and 1064 nm	Pd	8.92, 12.74, and 19.90 J/cm^2	3.56 to 8.91 nm
Inada et al. (2003)	Hydrogen gas	266 nm	Si	60 J/cm^2	5 nm
Pasha et al. (2010)	Acetone	1064 nm	Palladium		7 nm

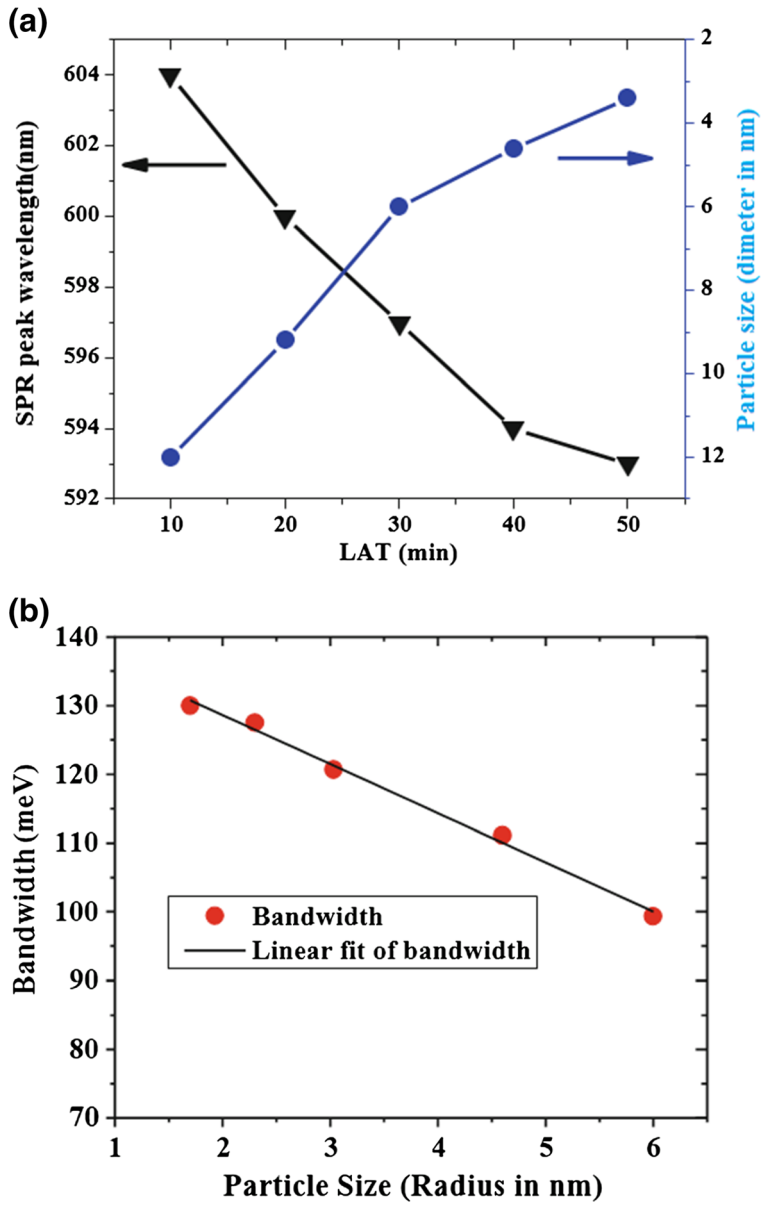

Fig. 5 Variations of SPR wavelengths and the average particle size (diameter in nm) as obtained from TEM micrograph analysis with the laser ablation time duration (min) are shown in **a**. Variation of the linewidth (meV) with the particle size (radius in nm) is shown in **b**. Symbols are experimental points and the solid line is the theoretically fitted line (Desarkar et al. 2012a)

the size of the particles (diameter in nm) in the context of the laser ablation time. TEM measurements reported decreased sizes with LAT, while the SPR peak exhibits a blue shift with ablation time. This peak is crucial towards the determination of the distribution of the size of the NPs. A Lorentzian fit was used to determine the Lorentzian linewidth (in meV) of the SPR peaks, as per Fig. 5b in the context of particle sizes. It is seen in Fig. 5b that the nanoparticle size is inversely proportional to the bandwidth, which implies intrinsic size effects.

As ablation time increases, NP production initially increases; however, this increase eventually plateaus. In reality, there is a build-up of NPs that shield the laser from the target, which is why no new NPs are generated after reaching its critical time (Desarkar et al. 2012a, b).

Effect of variation of laser pulse width on nanoparticle size

The pulse duration is an essential parameter in the synthesis of NPs. Altering it from nanoseconds (ns) to

Table 3 R&D on the effect of pulse widths and time durations on the synthesis of NPs

Author	Target	Fluence	Pulse widths and time durations	Particle size
Schwenke et al. (2011)	Silver, magnesium, and zinc	0.35 and 0.22 J/cm^2	Pulse width 7 ps and ablation times up to 60 min	Mean primary particle diameter, 15, 51, and 17
Desarkar et al. (2012b)	Sn	181 J/cm^2	Pulse width 10 ns and time duration of 10, 20, 30, 40, and 50 min	Average sizes (radius) varying between 3.2 and 7.3 nm
Al-Mamun et al. (2012)	Alumina	20 J/cm^2	Pulse width 6 ns and time duration 1–2 h	12 to 18 nm
Dadashi et al. (2015)	Bismuth	118 mJ/pulse	Pulse width 12 ns and time duration 5 min	Average size of 27 ± 9 nm
Popovic et al. (2014)	Si	4.4 J/cm^2 and 15.7 J/cm^2	Pulse width 150 ps and time duration 15 min	Size distribution 13 nm
Chaturvedi et al. (2017)	Ti	~ 5J/cm^2	Pulse width 5 ns and time duration 30 min, 60 min, and 90 min	The average size of ~ 50 nm
Aghdam et al. (2019)	Cu	Pulse energy of 40 and 100 mJ/pulse	Pulse width 10 ns and time duration 15 min and 25 min	The mean sizes of 40 and 80 nm

picoseconds (ps) and femtoseconds (fs) results in the ablation mechanism changing from melting and thermal evaporation to phase explosion, respectively. A shorter pulse duration results in a more efficient ablation process, resulting in instantaneous evaporation and a minimal heat-affected zone. In picoseconds, ablation was faster due to its lower than ns threshold for metals (Giorgetti et al. 2015a). It has also been reported that the energy absorbed by the target remains quite low in the case of ultra-short laser pulses. Consequently, utilizing ultra-short laser pulse durations of ps/fs is advantageous in that it can be used to increase the efficiency of the laser ablation process (Schwenke et al. 2011).

The production efficiency remains quite high relative to the shorter ps or long ns pulsed lasers for similar wavelengths (Stašić et al. 2016). Table 3 summarizes research works on the effect of time duration on the synthesis of NPs for multiple targets under different conditions.

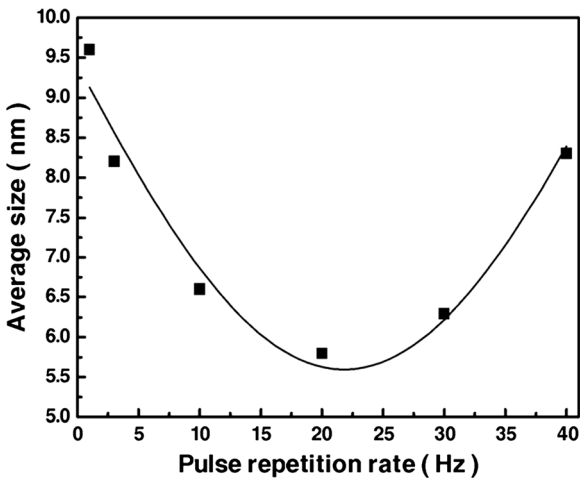

Fig. 6 The average size of nanoparticles in the films versus pulse repetition rate (Wang et al. 2007a)

Effect of pulse repetition rate

Wang et al. (2007a) examined the influence of pulse repetition rate (1 and 40 Hz) on the mean size of the nanocrystalline. The results from the Si films (nc-Si films) in high-purity Ar gas at a pressure of 10 Pa at room temperature is presented in Fig. 6.

The results confirmed the correlation between the mean size and pulse rate being 9.6 nm in 1 Hz, 8.5 nm in 3 Hz, 6.6 nm in 10 Hz, 5.75 nm in 20 Hz, 6.5 nm in 30 Hz, and 8.5 nm in 40 Hz. It was also confirmed that the smallest NPs that can be synthesized is at the optimum pulse rate and medium values. The influence of the repetition rate of laser pulses (RRLP) in 1–10 Hz on the synthesis of Ag nanoparticles (Ag-NPs) by laser ablation in ethanol was analyzed, and the ablation efficiency of Ag-NPs in liquid diminution with the reduction of

Table 4 R&D on the effect of laser fluence/energy density on the produced NPs

Author	Liquid	Target	Wavelength (λ)	Energy/ power	Energy density/fluence	Particle size
Chewchinda et al. (2014b)	Ethanol	P-type silicon wafer	532 nm, F = 10 Hz		0.15 to 0.45 J/cm^2	0.15 to 0.31 J/cm^2, from 0.01 to 0.08 mg and 0.45 J/cm^2 to 0.02 mg
Dorranian et al. (2014)	Acetone	Cu	1064 nm, F = 5 Hz		1, 1.5, 2, 2.5, and 3 J/cm^2	1–6 nm
Azadi Kenari (et al. 2018)	Ethanol	Ta	1064 nm, F = 10 Hz		0.3, 0.6, and 0.9 J/cm^2	12–18 nm
Zamora-Romero (et al. 2019)	DI water	Mo	1064 nm, F = 10 Hz		5 to 20 J/cm^2	48 to 141 nm
Giorgetti et al. (2015b)	Deionized water	Ti	1064 nm, F = 10 Hz		1.4–14 J/cm^2	
Kobayashi et al. (2013)	Ethanol	Si	532 nm		0.17 J/cm^2, 0.32 J/cm^2, 0.45 J/cm^2	6 mm
Ismail et al. (2018)	Ethanol	PbI_2	1064 nm, F = 1 Hz		2.7 to 5.4 J/cm$_2$	10 to 75 nm

the repetition rate of laser pulses from 1 to 10 Hz was reported (Valverde-Alva et al. 2016).

Effect of fluence/energy density

Laser ablation in liquid can be used to synthesize NPs at multiple energy densities. A higher energy density results in increased production of NPs (Al-Azawi et al. 2016; Takada et al. 2013). An example of this is when bulk Al was used as a target for the laser ablation technique (Nd:YAG laser with wavelength 1064 nm) to synthesize Al_2O_3 NPs. The suspension gets opaquer, which confirms the presence of Al_2O_3 NPs post-ablation. Laser energy influences and changes the particle sizes, fluctuating at ~ 20–100 nm. The predominant particle size remains small for energies of 1–5 J, while it becomes more significant for an energy of ~ 3 J. The downside of the former is the nonuniformity and aggregation of the synthesized NPs, while in the case of the latter, some of the NPs melted due to its exposure to high energy (Piriyawong et al. 2012). However, as energy density increased further, the self-absorption of NPs inhibited the ablation on the target. The nucleation and growth theory can be used to explain the size differences. At low-energy densities, nucleation was challenging, resulting in a small number of nuclei and bigger particles sizes, while at high-energy densities, nucleation took place simultaneously, leading to high quantities of nuclei and smaller particle sizes (Chewchinda et al. 2014a). It should also be pointed out that the size evaluation of the NPs via its bandgap energy originating from the extinction spectra of the colloids could be erroneous, which could be made even worse by the fact that the bandgap is a function of the size of the NP (Giorgetti et al. 2015b). It was also confirmed that the average size of the NPs is inversely related to the thickness of the targets (Scaramuzza et al. 2015). Table 4 summarizes the literature on the influence of laser fluence/energy

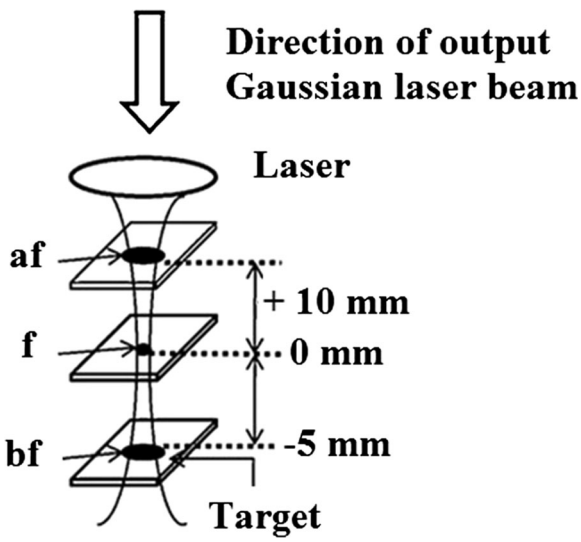

Fig. 7 Laser spot size area variation (af above focus, f focus, bf below focus) (Nath et al. 2011)

Table 5 R&D on the effect of focusing conditions on the produced NPs

Author	Liquid	Target	Focal length lens	Spot size	Fluence	Wavelength	Particle size
Nath et al. (2011)	Distilled deionized water	Titanium	5 cm	~ 600, 80 and 400 μm	80 J/cm^2, 1.4 J/cm^2, and 0.2 J/cm^2	532 nm	13, 12, and 9 nm
Elsayed et al. (2013)	Deionized water and ethanol	Gold	5 cm	600, 150, and 500 μm μm	280, 70, and 18 J/cm^2	1064 nm	9, 10, and 18 nm
Nikov et al. (2013)	Double distilled water	Au		1.1 mm	15.5 J/cm^2	1064, 532, and 355 nm	22.2 and 14.7 nm λ = 1064 nm 10.7 and 4.3 nm when λ = 532 nm 9.5 and 3.6 nm when λ = 355 nm
Dorranian et al. (2014)	Acetone	Cu	80 mm	40 μm	1, 1.5, 2, 2.5, and 3 J/cm^2	1064 nm	1–6 nm
Baruah et al. (2018)	Distilled water	Ag	25 cm	~ 3.12 × 10–3 cm^2	30, 50, and 70 mJ	532 nm	15, 13, and 10 nm
Díaz-Núñez et al. (2017)	Pure water	Silver	25 cm	100 μm	10.2–25.5 J/cm^2	800 nm	21 to 40 nm
Sapkota et al. (2017)	Deionized water	Tin		~ 100 μm	~ 50 J/cm^2	351 nm	30 to 50 nm
Haram and Ahmad (2013)	Distilled water	Cu	50 cm	2 mm	5.73–9.87 J/cm^2	1064 nm	2–55 nm
Kulinich et al. (2013)	Deionized water	Zn	3 cm		30 mJ/pulse	532 nm	50 to 100 nm
Hidayah et al. (2018)	Distilled water	Au–Ag	10 cm		2.1 W	800 nm	The size of Au–Ag nanoalloys of around 15.03 nm
Kim et al. (2014)	Deionized water	Pd	250 mm	0.8 and 1 mm	8.92, 12.74, and 19.90 J/cm^2	355, 532, and 1064 nm	3.56 to 8.91 nm
Starinskiy et al. (2017)	Distilled deionized water	Au		~ 1 mm	3–10 J/cm^2	1064 nm	~ 10 nm

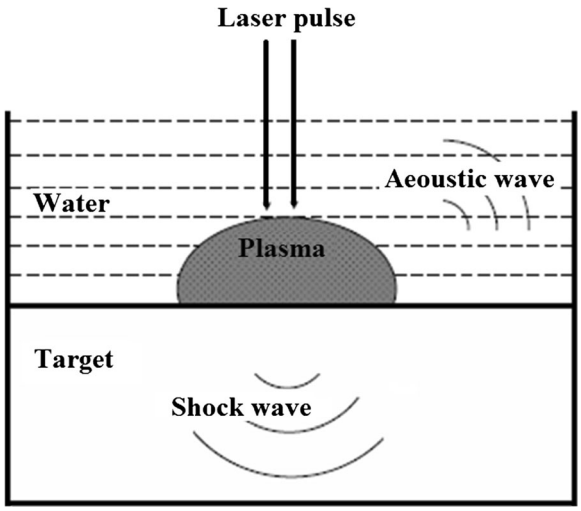

Fig. 8 A scheme showing the acoustic waves propagation in the confining liquid (liquid and the shock waves generation inside the solid target) (Messina 2011)

density on the synthesized NPs for multiple targets under different conditions.

Effect of Laser focusing parameters on produced NPs

Effect of focusing conditions

Another critical factor that influences the size of the NPs and its corresponding deviations is the set of focusing conditions (Elsayed et al. 2013). The targets were ablated under multiple focusing conditions by altering the position of the lens via a micrometer (μm) screw that comes attached with the lens' mount. The target is fixed and ablated for three positions: above, below, and at the focal point, as per Fig 7.

Focusing conditions represents an important parameter that is crucial towards the synthesis of small size NPs with a narrow distribution. It not only alters the fluence, but it also changes the degree of ionization of the liquid medium containing the colloids. Table 5 summarizes research works on the effect of focusing parameters on the synthesis of NPs for multiple targets under different conditions.

Plasma plume status and produced NPs

A typical plasma plume can be seen during irradiation, as per Fig. 8. When laser ablation is carried out within a liquid medium, the confinement induced by the liquid upon the submerged ablated solid target results in the creation of the shock wave within the plasma plume. The plasma produced by the laser tends to expand at supersonic velocity; however, this expansion creates shock waves, as the liquid curtails the supposed expansion. The impingement of the laser on the submerged solid target results in the continuous presence of ablated material within the plume, culminating in a plasma-intense luminosity. The vaporized species are classified as highly excited ionic particles that will incoherently relax to its original quantum states, emitting electromagnetic radiations, as illustrated in Fig. 8. This emission process differs from the ones taking place in a laser resonator because light emission from the plume is spontaneous instead of being coherently stimulated. The plasma looks like it is strongly illuminated, which can be attributed to the incoherent emissions (Messina 2011).

It is shown that the most intense plasma is generated by installing the target at a point slightly prior to the geometric focal point.

The intensity of the plasma is correlated to the amount of ablated material, and the mean size of NPs is linked to the second highly dispersed distribution of NPs. This implies the involvement of plasma-related processes in the ablation of material, the result of which is the formation of relatively large particles (De Giacomo et al. 2014; Sylvestre et al. 2005). It is also evident that plasma parameters are unaffected by pressure; however, uniform magnetic external fields do affect the NPs, which magnetically confines the plasma to a smaller region, resulting in an increase in its density (Singh et al. 2017b).

Effect of medium of ablation ambient on produced NPs

Effect of liquid environment on NPs size

The liquid phase laser ablation technique can be used to control the size of the NPs via changing the laser's parameters, such as laser fluency {(energy density), pulse width and time duration, and wavelength and repetition ratio}, laser focusing parameters {focal length and the target position}, and the medium of ablation ambient {fluid type, pressure, solvent, plasma plume}. Furthermore, the average particle sizes of the colloidal NPs are inversely related to the depth of the liquid (Al-Azawi

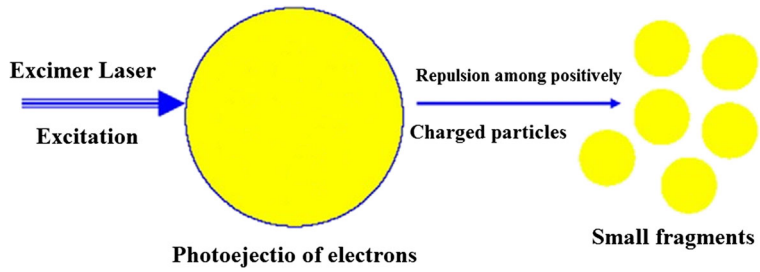

Fig. 9 Mechanism of photofragmentation process (Badr and Mahmoud 2007).

et al. 2016). Increasing liquid temperature alters the morphology of the nanomaterial, from spherical into elongated (Al-Dahash et al. n.d.). The morphological change can be attributed to the increase in the kinetic energy increasing the collision rates between the initially formed large NPs from the condensation process and the NPs that are present in the path of the laser beam. The fragmentation from these collisions could further, in theory, reduce the size of the NPs. Additional irradiation of laser pulses onto colloidal solution via liquid-phase laser ablation can also be used to decrease the size of the NPs. The NPs undergo photo fragmentation post-laser excitation, resulting in smaller fragments of NPs; this mechanism is detailed in Fig. 9 (Badr and Mahmoud 2007).

Controlling the particle size is a crucial aspect of colloidal synthesis, as the physico-chemical properties of the nanometallic particles are very much reliant on their sizes. An example of this can be seen in the case of the colloidal solutions of the Ag NPs prepared in deionized water (DIW), ethanol, and polyvinylpyrrolidone (PVP) via ablation with 1064 nm lasers to elucidate the effect of a liquid medium on the average particle size, average particle size distribution, ablation efficiency, and stability. The results are tabulated in Table 6.

Changing the liquid medium from deionized water, ethanol, and polyvinylpyrrolidone results in changes to the average particle size of the NPs (Al-Azawi et al. 2016). The application of a magnetic field during the laser ablation process increased the concentration and sizes of the NPs, resulting in increased absorbency, efficiency, and optical parameters. However, externally applied electric field decreased the size of the resulting NPs, examples include the particle size of smaller NPs of Sn or Au created under different electric fields (Sapkota et al. 2017). Table 7 summarizes previous research on the effect of laser ablation in liquid on the size of synthesized NPs for multiple targets under different conditions.

Effect of liquid medium on NPs shape

It was also confirmed that solvents (ethanol, deionized water, and acetone) used in the laser ablation method affect the shape of the synthesized NPs.

It can be seen that the solvent control, not only the shape, size, and distribution of the synthesized NPs, but also its composition (Bajaj and Soni 2009). This can be seen in the case of Sn produced by pulsed laser ablation in liquid, where its mean size, distribution, and shape are shown in Fig. 10.

The ablation of NPs relies upon two mechanisms: (1) direct nucleation of atoms in the condense plume and (2) NPs act as growing centers for the incoming species. The effect of the mechanism resulted in wide size distribution.

Packed and stronger bonds are attracted to the surface via highly polar molecules. The electrostatic repulsive force from the overlapping electrical double layers of the nuclei and species in the plume preclude further growth, aggregation, or precipitation. An example of

Table 6 The average size, ablation efficiency, and particle size distribution of Ag NPs prepared in the three different solutions of PVP, deionized water, and ethanol (Al-Azawi et al. 2016)

Liquid medium	Average particle size (nm)	Ablation efficiency	Particle size distribution	Stable and suspension
PVP	16.36 ± ±7.34	High	Narrower	Yes
DIW	22.88 ± ±9.46	Low	Broad	Yes (modest)
Ethanol	26.44 ± ±12.10	Lowest	Narrow	No

Table 7 R&D on generating NPs using different liquids

Author	Fluid	Target	Time	Fluence	Particle size
Zamiranvari et al. (2017)	CTAB	ZnO	Pulse width of 7 ns		18.9 to 52.3 nm
Amans et al. (2011)	2-[2-(2-methoxyethoxy) ethoxy] acetic acid (MEEAA)	$Y_2O_3:Eu^{3+}$, $Gd_2O_3:Eu^{3+}$, and $Y_3A_{15}O_{12}:Ce^{3+}$	Pulse width Δt = 5 ns		2 and 4.5 nm
Bajaj and Soni (2009)	Deionized water, acetone, and ethanol	Tin	Pulse width 5 ns	2.3–10.5 J/cm^2	2 and 37 nm
Chewchinda et al. (2013)	Ethanol	Si	Pulse width 10 ns		6.98 and 3.01 nm
Dewalle et al. (2011)	Acrylic paint	Al	Pulse width 5 ns	0.1 to 11 J/cm^2	10–15 nm
Wang et al. (2009)	Gas N_2 (99.5%)	Fe	Pulse width 0.5 and 2.0 ms		18 to 33 nm
Tilaki and Mahdavi (2007)	Deionized water with various concentrations of ethanol	Gold	Pulse width 10 ns	1.1 J/pulse/cm^2	2–99 nm
Haram and Ahmad (2013)	Distilled water	Cu	Pulse width 5–6 ns	5.73–9.87 J/cm^2	2–55 nm
Moura et al. (2017)	DDW, acetone, and ethanol	Ag	Pulse width 35 ns	2122.2, 3183.3, and 4244.0 J/cm^2	11.8, 13.9, and 17.7 nm
Soliman et al. (2011)	Distilled water	Ti		22.4 J/cm^2	140 to 310 nm
Amagasa et al. (2017)	Ethanol	Fe_3C	Pulse width 5 ns	Pulse energy 100 mJ	5–100 nm

this is the impact of the liquid utilized in the PLA of Sn. The dipole moment is imperative, with acetone's being much higher than that of deionized water or ethanol. A significant dipole moment results in smaller average sizes since the first mechanism is suppressed. It is also more likely that the NPs turn out spherical (Bajaj and Soni 2009). The mean size, size distribution, and shape of particles obtained via different liquid mediums are tabulated in Table 8.

The metal NPs exhibited a spherical morphology in all of the solvents (Al-Azawi et al. 2016). NPs can be synthesized into nanopowders or colloids via laser ablation with a solid target submerged in a liquid and gaseous surrounding. The physico-chemical properties of the synthesized NPs can be tailored via the parameters of laser ablation in the liquid medium (Aye et al. 2014). Laser ablation in a stirred liquid medium is more effective relative to a static liquid medium, as evidenced by the increased ablation yield (by 30%) and improved repeatability and quality of the resulting colloidal properties (Resano-Garcia et al. 2015). Table 9 summarizes previous research works on the effect of liquid medium on the synthesized NPs for multiple targets under different conditions.

Effect of ambient gas on formation process of NPs

Surface morphology analyses of the synthesized NPs showed that the average mass and volume of the NPs prepared in different gaseous mediums initially increased and then decreased in tandem with the distance between the target and the substrate (Wang et al. 2007b). The room temperature production via laser ablation results in agglomerated particles in the gaseous phase. The formation of the NPs is dependent upon the occurrence of random collisions, which makes controlling the size distribution, crystallinity, shape, and the temperature of the process a complicated undertaking (Tsuji et al. 2012a).

For example, in preparing Si nanoparticles (Muramoto et al. 1999), increasing the ambient pressure for He from 1 to 10 Torr changes the diameter of the resulting NPs from 10 to 25 nm. The same effect can be obtained with Ar but in a less pronounced manner. The dispersion and size distribution increases with He pressure but not with Ar. Plume confinement, which is an essential factor in production, is also affected by ambient gas.

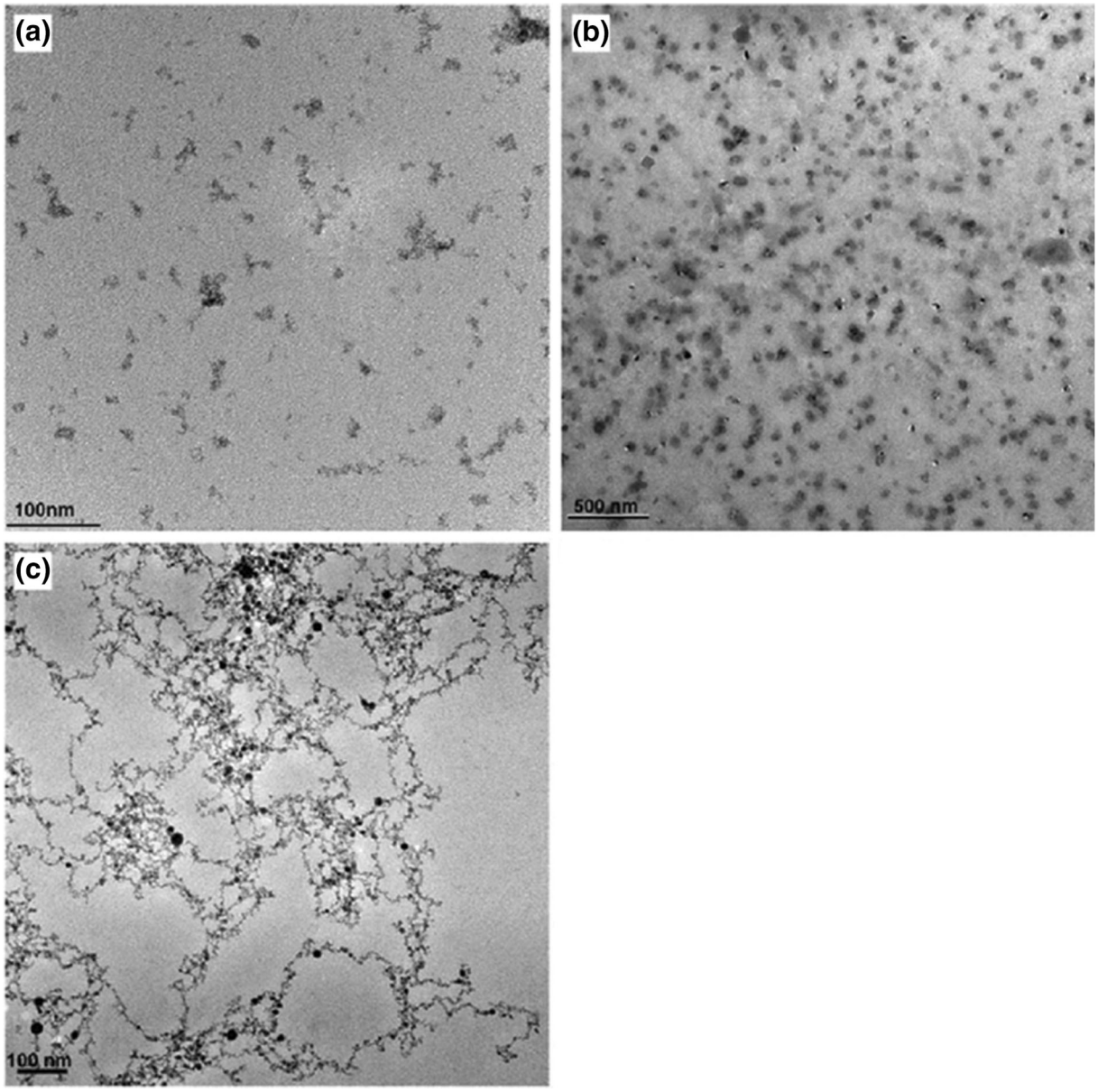

Fig. 10 TEM micrographs of synthesized NPs prepared at the laser fluence of 2.3 J/cm^2 in **a** ethanol, **b** deionized water, and **c** acetone (Bajaj and Soni 2009).

Ar is heavier than He; therefore, it offers greater confinement of plumes. Usually, Ar contains a much more densely packed Si plume, which means its production is quicker (Muramoto et al. 1999). Table 10 summarizes the previous researches in the literature discussing the effect of ambient gases on the formation process of NPs for different targets under different work conditions.

Effect of pressure

Kulinich et al. (2013) investigated the influence of pressure on medium in PLA on NPs synthesis. They applied different pressures to explore changes in medium pressure on laser ablation of Zn and the preparation of ZnO NPs.

The PLA of Zn in distilled water at varied pressures (from 0.1 to 31 MPa) generated ZnO nanocrystals. The

Table 8 Calculated size, size distribution, and observed shape of the NPs prepared by laser ablation in different liquid media (Bajaj and Soni 2009)

Liquid	Dipole moment (D)	Average size (nm)	Size distribution (nm)	Shape
Ethanol	1.69	–	–	Thread-like
Deionize water	1.85	37	± 10	Elongated
Acetone	2.89	2	± 1	Spherical

results (Fig. 11) show that at elevated medium pressures, smaller NPs with uniform size distribution and stronger green luminescence were produced (Kulinich et al. 2013).

Table 11 summarizes the previous researches in the literature discussing the effect of pressures on the synthesized NPs for different targets under different work conditions.

Table 9 The effect of liquid medium on NP shape

Author	Liquid	Wavelength	Target	Shape
Amans et al. (2011)	2-[2-(2-Methoxyethoxy) ethoxy] acetic acid (MEEAA)	355 nm, F = 10 Hz	Y_2O_3:Eu^{3+}, Gd_2O_3:Eu^{3+}, and $Y_3Al_{15}O_{12}$:Ce^{3+}	Crystallize
Al-Mamun et al. (2012)	Distilled water	1064 nm, F = 10Hz	α-Al_2O_3	Spherical
Chewchinda et al. (2014a)	Ethanol	532 nm, F = 10 Hz	P-type silicon wafer	Spherical
Chewchinda et al. (2013)	Ethanol	1064 and 532 nm, F = 10 Hz	P-type h100i silicon wafer	Crystal
Johny et al. (2019)	Acetone, isopropanol, and dimethyl formamide	532 nm, F = 10 Hz	SnS_2	Spherical particles
Popovic et al. (2014)	Deionized water	1064 nm, F = 10 Hz	Silicon	Spherical or nearly spherical in shape
Nikov et al. (2013)	Double distilled water	1064, 532, and 355 nm, F = 10 Hz	Gold	Spherical and sphere-like shaped
Hu et al. (2011)	Distilled water and 0.01 M sodium dodecyl sulfate (SDS) solution	1064 nm, F = 20 Hz	Zinc and ZnO	Spherical shapes
Kobayashi et al. (2013)	Ethanol	532 nm, F = 10 Hz	Silicon	Spherical
Aye et al. (2014)	Distilled water, absolute ethanol, and acetone	1064 nm, F = 30 kHz	Iron	Spherical
Chakif et al. (2014)	Water, acetone, and water/acetone	1030 nm, F = 100 kHz	Fe	Spherical
Gondal et al. (2013)	Deionized water and hydrogen peroxide	532 nm, F = 10 Hz	Copper	Spherical shape
Ismail and Fadhil (2014)	Distilled water	1064 nm, F = 1 Hz	Bismuth	Polycrystalline
San et al. (2014)	Deionized water	527 nm, F = 1 kHz	Sugar beet bagasse	Nanocrystal
Kim et al. (2013)	Deionized water	266, 355, 532, and 1064 nm, F = 10 Hz	Gold	Nanocrystal
Nath et al. (2011)	Deionized water	532 nm, F = 15 Hz	Titanium	Perfectly spherical
Kim et al. (2014)	Deionized water	355, 532, and 1064 nm, F = 10 Hz	Pd	Homogeneous spherical palladium
Desarkar et al. (2012b)	Pure deionized water	1064 nm, F = 10 Hz	Solid Sn	Spherical
Swarnkar et al. (2011)	Double-distilled water	1064 nm	Copper	Cactus-like structure
Takada et al. (2013)	Distilled water	1064 nm, F = 32 kHz	Au or Zn	Spherical or crystalline

Table 10 The effect of ambient gas on formation process on the produced NPs

Author	Gas	Pressure	Target	Fluence	Particle size	Shape
Muramoto et al. (1999)	He and Ar	1 to 10 Torr	Si	2.6 J/cm^2	Mean of diameter (10 to 12.6 nm)	Spherical
Wang et al. (2007b)	Argon gas	10 Pa	Si			Crystalline
Tsuji et al. (2012a)	Air	0.1 MPa	Ti		Particle diameter of 11–45 nm	Spherical
Dewalle et al. (2011)	Acrylic paint and gas (air)	7 bar	Al	0.1 to 11 J/cm^2	10–15 nm	Spherical particles
D'Andrea et al. (2009)	Ar gas	70 Pa	Ag	Energy density = 2.0 J/cm^2	The average size of 2.8 nm	Ag film
Almeida et al. (2012)	He and Ar gas		PbTe			Film
Wang et al. (2009)	Gas N_2 (99.5%)	0.05 MPa	Fe		18 to 33 nm	Spherical in shape and they form a chain-like structure
Ramanujan and Rawat (2006)	Argon	0.5–7.5 kPa	Iron cobalt (FeCo)		65 to 120 nm	Island-like
Chu et al. (2010)	Pure Ar gas	1 to 200 Pa	Si	3 J/cm^2		Crystalline films
Wang et al. (2007a)	(99.9995%) Ar gas	10 Pa	Si	4 J/cm^2		Nanocrystalline Si films
Orii et al. (2007)	Argon gas	1.3 kPa	ZnTe		Approximately 15 and 22 nm	Spherical
Inada et al. (2003)	Hydrogen	5–530 Pa	Si	60 J/cm^2	Approximately 5 nm	High porosity structure
Hamoudi et al. (2012)	He	5 Torr	Pt	4 J/cm^2	Particle average diameter 1.4 nm ± 0.8 nm	Thin film catalysts
Tsai et al. (2006)	Oxygen	7 to 11 GPa	Zr		2, 6, and 18 nm	Chain aggregates
Ma et al. (2011)	O_2/He mixed gas atmosphere	0.5 to 1.8 kPa	ZnO		~ 10 nm	Highly crystalline
Riabinina et al. (2010)	He	10^{-5} to 11 Torr	Platinum	8 J/cm^2	25 to 5 nm	Crystallite
Hirasawa et al. (2004)	He	1000 Pa	Si		5 to 13 nm	Spherical shape
Ou et al. (2008)	N_2/O_2	0 and 200 kPa	Zn		~ 60 nm	Crystalline structure nearly identical

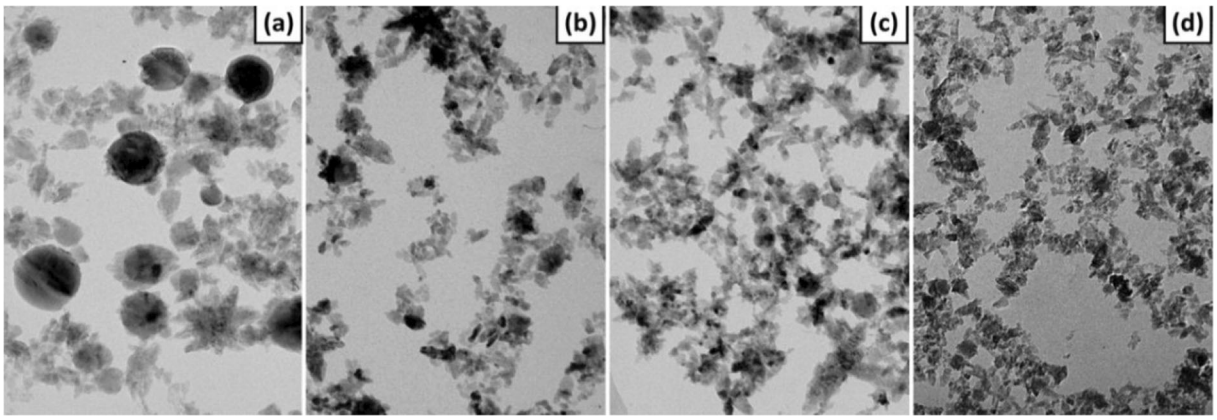

Fig. 11 TEM images presenting ZnO NP morphology as a function of pressure. **a** Atmospheric pressure, **b** 15 MPa, **c** 22 MPa, **d** 31 MPa (Kulinich et al. 2013)

Lessons and insights learned

Laser pulse parameters

Laser ablation in a liquid was used to prepare metallic NPs at multiple energy densities. Higher energy densities resulted in increased yields of NPs. However, further increasing the energy density will inhibit the ablation of the metal target due to the self-absorption of NPs. The nucleation and growth theory can be used to explain the size differences at multiple energy densities. At low-energy densities, nucleation is difficult, resulting in smaller amounts of nuclei and larger particle sizes, while at higher energy densities, nucleation coincides, leading to a large number of nuclei and smaller particle sizes. Increasing energy density decreases the size of the NPs up to their critical size.

Pulse width and time duration are crucial towards the size and distribution of the NPs. Table 12 tabulates the optimum pulse widths and time durations needed to produce the smallest NPs for multiple targets via laser ablation.

The particle size of colloids can be tuned using laser wavelengths, from 1064 to 355 nm. Generally, higher wavelengths result in increased efficiency and finer spherical particles. The pulse repetition rate can change the average size of the NPs, where it is a nonlinear dynamic process of PLA. The standard pulse repetition rate reported in the literature is 10 Hz.

NA not available

Laser focusing parameters

The focusing conditions (i.e., target position) are vital towards the formation of a narrow distribution of the size of the NPs. The distance between the lens and the target dictates the spot size on the target. The focal length affects the shape and size distribution of the NPs. A minimum spot

Table 11 The effect of pressure on the produced NPs

Author	Fluid	Pressure	Target	Particle size
Kulinich et al. (2013)	Deionized water	(0.1, 6.5, 15.4, 22.4, and 30.1 MPa)	Zn	50 to 100 nm
Soliman et al. (2011)	Water	0.1, 3, and 30 MPa	Ti and Zn	
Chu et al. (2010)	Pure Ar gas	1 to 200 Pa	Si	
Riabinina et al. (2010)	Helium gas	10−5 to 11 Torr	Platinum	25 to 5 nm
Hamoudi et al. (2012)	He background gas	1, 2, 4 to 5 Torr	Pt catalysts	
Muramoto et al. (1999)	He and Ar	1 to 10 Torr	Si	Mean of diameter (10 to 12.6 nm)
Tsuji et al. (2012a)	Air	0.1 MPa	Titanium	Particle diameter of 11–45 nm
Dewalle et al. (2011)	Air	7 bar	Al	10–15 nm

Table 12 Optimum pulse width and time duration to produce minimum nanoparticle size for different targets as reported in literature

Target {used pulse width and time duration) at different case studies}	Recommended pulse width and time duration	Nanoparticle size
Si/(13 ns, 30 min), (13 ns,30 min), (13 ns, 30 min), (10 ns, 30 min), (120 ps,15 min), (15 ns, NA), (NA,10 min), (15 ns, NA), (10 ns, NA), (15 ns,4 h), (8 ns, NA)	Pulse width 13 ns, and irradiated for 30 min	6 nm
Cu/(5–6 ns, NA), (7 ns, NA), (5 ns, 15 min), (NA, 30 min), (NA, 15 min)	Pulses of 5 ns, and ablation time 15 min	10 nm
Au/(NA, 15 min), (5 ns, 15 min), (5–7 ns, 20 min), (10 ns, 8 min), (120 ps, 20 min), (NA, 5 min), (15 ns, 20 min), (10 ns, 5 min), (10 ns, 20 min), (7 ns,10 min), (500 fs, NA)	Pulses of 5 ns and ablation time 15 min	Average sizes of approximately 5.0 nm
Ag/(NA, 10 min), (10 ns, 30 min), (7 ns, NA), (7 ns, 4 min)	Pulse width was 7 ns and ablated for 4 min	16.77, 26.76, and 32.24 nm
Al/(5 ms, NA), (6 ns, 10 min), (5 ns, NA), (6.1 ns–2 h)	Laser pulses of 6 ns, duration 10 min	Smaller than 100 nm in diameter, mostly ~ 40–50 nm
Zn/(7 ns, 60 min), (5 ns, 90 min), (6 ns, 1.5–3 h), (8 ns, 60 min), (2 ms, NA)	Pulse width was 8 ns and irradiation time 60 min	2.8, 3.3, 3.7, and 4.7 nm
Ti/(5 ns, 30 min), (25 ns and 25 ps, NA), (6 ns, NA)	Pulse duration of 5 ns and irradiation time was 30 min	9, 12, and 13 nm
Pt/(6 ns, 1 h), (15 ns, NA), (17 ns, 1 h)	Pulse width was 17 ns and irradiation time 1 min	2.4 nm
Fe/(3 ns, 7 min), (300 fs, NA), (0.5 and 2 ms, NA)	Pulse duration of 3 ns and irradiated for 7 min	The mean particle size of 20 nm

size is dependent upon the focal length, which alters the fluence, resulting in NPs with multiple shapes and sizes.

A typical plasma plume is detectable during laser irradiation. If the target lies just under the focal point, an intense plasma is created. At low laser energies, the targets' temperature increases, but its vaporization rate is curtailed due to liquid acting as a confiner at its surface, which scuttles the formation of plumes. At an intermediate laser beam energy, the plume is formed slowly, while under high energies, the laser ablation of the target in the liquid medium resulted in the production of plasma plume that is visible to the naked eye (emitting a noticeable noise) near the target surface, which could be due to the breakdown of the cavitation bubble being formed from the vaporization of the fluid layer that is in close contact with the plasma. Plasma

Table 13 Appropriate ambient gases used for different targets as learned from the literature

Target/{used gases at different case studies}	Recommended gases	Pressure	(Minimum) mean NP size and NP shape	Remarks
Si/{H, He, Ar, (He, Ar)}	He or Ar	1 to 10 Torr	10 to 25 nm, spherical	Nanoparticle distribution in an ambient He gas was different from that in ambient Ar gas
Zn/Mixed O_2/N_2	Mixed O_2/N_2 gas	150 kPa was added to fixed 100 kPa background oxygen.	~ 60 nm, crystalline structure	Size distribution of 10–100 nm at room temperature
Ti/Air	Air	0.1 MPa	Particle diameter of 11–45 nm, spherical	The primary particles diameter increases with temperature
Pt/He	He	1 to 5 Torr	4.4 to 5 nm, very smooth and dense	He pressures increased, the surface roughness increased
Fe/N_2	N_2	0.05–0.25 MPa	18 to 33 nm	The target size has a large effect on the nanoparticle

emission and the corresponding sounds near the focal point are much higher. Counterintuitively, the most exceptional sound and emission are produced when the target lies just prior to the focal plane, where the size of the NPs increases.

Medium of ablation ambient

Pulsed laser ablation deposition (PLAD) in an ambient gas has been widely used to synthesize NPs and can be controlled via the type of ambient gas, pressure, and the position of the substrate collecting the NPs. Pressure is the best variable when it comes to manipulating the size of the NPs; however, complete size control is complicated due to the randomness of gaseous collisions. Its temperature is especially challenging to control. Coalescence is the primary factor in deciding the primary NPs' diameter. A summary of the most appropriate ambient gases for different targets is tabulated in Table 13.

Pulse laser ablation in liquids (PLAL) is suitable for the synthesis of NPs. The effects of ambient liquids on the synthesized NPs and solvent media (distilled water, ethanol, and acetone) can result in various sizes, shapes, compositions, and crystal structures. It was shown that laser ablation of many noble metals within solvents results in colloidal settles of these metals. For example, when using Cu as a target, submerging it in acetone instead of water results in smaller NPs at a lower fluence and the lack of oxidation. The suitability of solvents, along with their prospects and limitations for multiple targets are tabulated in Table 14.

Table 14 Appropriate solvents used at different targets as learned from the literature

Target/{used liquids or solvents at different case studies}	Recommended liquid/solvent	Shape	Remarks
Si/{(deionized water), (ethanol)}	Ethanol	Spherical or nearly spherical	Besides silicon NPs, silicon oxide NPs presented.
Cu/{deionized water and hydrogen peroxide}(deionized water), (acetone)	Acetone	Spherical	The production is Cu NPs without oxidization
Au/(ethanol), (deionized water), {LiCl, NaCl, KCl, NaBr, and NaI added to deionized water}, {ethanol, deionized water and mixture of deionized water and ethanol}	Ethanol, deionized water	Spherical	In ethanol increased the larger particles but in the water smaller particles
Ag/{(chlorides (NaCl, KCl) or iodides (NaI, KI) added to Neat water)}, (deionized water), (acetone)	Acetone, deionized water	Spherical	The mean diameter from 12 to 29 nm in deionized water. The average size from 12.99 to 32.24 nm in acetone.
Al/(ethanol), (deionized water)	Ethanol	Spherical	In ethanol without oxidation
Zn/{HCl, NaOH, HCl, deionized water}, deionized water, {distilled water, sodium dodecyl sulfate (SDS)}, {hydrogen peroxide pure H_2O_2, and H_2O_2 mixed with sodium dodecyl sulfate (SDS), cetyltrimethylammonium bromide (CTAB) and octaethylene glycol monododecyl ether (OGM)}	{Hydrogen peroxide pure H_2O_2, and H_2O_2 mixed with sodium dodecyl sulfate (SDS), cetyltrimethylammonium bromide (CTAB) and octaethylene glycol monododecyl ether (OGM)}	Grain	The grain sizes measured were 4.7, 3.7, 3.3, and 2.8 nm in pure H_2O_2 and H_2O_2 mixed with SDS, CTAB, and OGM
Ti/deionized water	Deionized water	Perfectly spherical	With titanium dioxide
Pt/deionized water	Deionized water	Spherical	The most homogeneous Pt
Fe/(distilled water), (ethanol), (acetone)	Distilled water, ethanol and acetone	Spherical nanoparticles were observed for all solvents	The colloidal stability of the nanoparticles is the highest in acetone, but the least in ethanol

Conclusion

This work encompasses details on the optimal synthesis of NPs reported in the literature, such as laser pulse parameters, laser fluency, laser focusing parameters, and the medium of ablation ambient.

The following conclusions are made:

The laser ablation method is a superior method with minimal side effects for synthesizing NPs. Many types of NPs can be produced using this method. The liquid medium at room temperature affects the shape, size, and distribution of the NPs colloidal/solutions for multiple targets, while also dictating the composition of the NPs.

The gas media of a solid target placed in a vacuum chamber is regarded as a versatile deposition method for the growth of thin films from almost any kind of solid target materials.

The threshold values and optimum working conditions of the parameters are vital towards the success of material ablation in the context of the particulates, atoms, and ions, and consequently, the optimum synthesis of NPs.

The energy density and size of the NPs are inversely related, up to a critical point, after which the size of the NP cease to be a function of energy density. It was also confirmed that both the pulse width and time duration are crucial factors towards the formation and size distribution of the NPs. The particle size of the colloids can be customized using laser wavelengths of 1064–355 nm, with higher wavelengths resulting in increased efficiency and better defined spherical particles. The rate of pulse repetition can be used to alter the size of the NP, the influence of which was determined to be a nonlinear dynamic process of the PLA. The standard pulse repetition rate is reported to be ~ 10 Hz. The focus parameters were tested at multiple distances close to the focal point to determine the distances above and below the focal point for making small adjustments; the convex lens of focal length between 30 and 100 mm is oft-cited in literature. In terms of the ambient medium of ablation, there are multiple control variables when utilizing ambient gases, such as the type, pressure, and position of the substrate gathering the NPs. Pressure represents the most straightforward factor that can be used to change the size of the NPs. For ambient liquids, different solvent media (distilled water, ethanol, and acetone) result in different sizes, shapes, compositions, and crystal structure of the synthesized NP. Finally, the optimal working conditions and values of the parameters are vital towards the success of ablation in forming NPs.

Acknowledgments Center of Research Excellence in Renewable Energy, Research Institute, King Fahd University of Petroleum & Minerals, Dhahran, 31261, Saudi Arabia is acknowledged. MA Alghoul and MK Hossain acknowledge the funding support provided by the King Abdullah City for Atomic and Renewable Energy (KACARE), Saudi Arabia through projects KACARE182-RFP-09 and KACARE182-REF-07.

Compliance with ethical standards

Conflict of interest The authors declare that they have no conflict of interest.

References

Aghdam HD, Azadi H, Esmaeilzadeh M, Bellah SM, Malekfar R (2019) Ablation time and laser fluence impacts on the composition, morphology and optical properties of copper oxide nanoparticles. Opt Mater 91:433–438

Ahmed N, Darwish S, Alahmari AM (2016) Laser ablation and laser-hybrid ablation processes: a review. Mater Manuf Process 31:1121–1142

Al-Azawi MA, Bidin N, Bououdina M, Abbas KN, Al-Asedy HJ, Ahmed OH, Thahe AA (2016) The effects of the ambient liquid medium on the ablation efficiency, size and stability of silver nanoparticles prepared by pulse laser ablation in liquid technique. J Teknol 78:7–11

Al-Dahash G, Obaid NM, Majeed HA The effect of liquid environment and magnetic field on optical properties of Pt nanoparticles colloidal prepared by pulsed laser ablation. Int J ChemTech Res 9:118–130

Ali FR, Mallipeddi R, Craythorne EE, Sheth N, Al-Niaimi F (2016) Our experience of carbon dioxide laser ablation of angiofibromas: case series and literature review. J Cosmet Laser Ther 18:372–375

Al-Mamun SA, Nakajima R, Ishigaki T (2012) Effect of liquid level and laser power on the formation of spherical alumina nanoparticles by nanosecond laser ablation of alumina target. Thin Solid Films 523:46–51

Almeida D, Rodriguez E, Agouram S, Moreira R, Cesar C, Jimenez E, Barbosa L (2012) Influence of the growing parameters on the size distribution of PbTe nanoparticles produced by laser ablation under inert gas atmosphere. In: SPIE LASE. International Society for Optics and Photonics, pp 82450K-82450K-82459

Amagasa S, Nishida N, Kobayashi Y, Yamada Y (2017) Effect of laser irradiation on iron carbide nanoparticles produced by laser ablation in ethanol. Hyperfine Interact 238:83

Amans D et al (2011) Synthesis of oxide nanoparticles by pulsed laser ablation in liquids containing a complexing molecule: impact on size distributions and prepared phases. J Phys Chem C 115:5131–5139

Arevalo R Jr, Bellucci J, McDonough WF (2010) GGR biennial review: advances in laser ablation and solution ICP-MS from 2008 to 2009 with particular emphasis on sensitivity

enhancements, mitigation of fractionation effects and exploration of new applications. Geostand Geoanal Res 34:327–341

Auciello O (1991) A critical review of laser ablation-synthesis of high temperature superconducting films. Mater Manuf Process 6:33–52

Aye HL, Choopun S, Chairuangsri T (2014) Influence of solvents on characteristics of nanoparticles prepared by pulsed laser ablation on iron target

Azadi Kenari F, Moniri S, Hantehzadeh MR, Dorranian D, Ghoranneviss M (2018) Fabrication of Ta nanoparticles induced by nanosecond laser ablation in ethanol: the study of laser fluence effects. J Mod Opt 65:899–906

Badr Y, Mahmoud M (2007) Excimer laser photofragmentation of metallic nanoparticles. Phys Lett A 370:158–161

Bajaj G, Soni R (2009) Effect of liquid medium on size and shape of nanoparticles prepared by pulsed laser ablation of tin. Appl Phys A 97:481–487

Barefoot R (2004) Determination of platinum group elements and gold in geological materials: a review of recent magnetic sector and laser ablation applications. Anal Chim Acta 509: 119–125

Baruah PK, Sharma AK, Khare A (2018) Effect of laser energy on the SPR and size of silver nanoparticles synthesized by pulsed laser ablation in distilled water. In: AIP Conference Proceedings, vol 1. AIP Publishing, p 050036

Chakif M et al Impact of solvent mixture on iron nanoparticles generated by laser ablation. In: SPIE BiOS, 2014. International Society for Optics and Photonics, pp 895507-895507-895509

Chan G, Mamut A, Martin P, Welk B (2016) Holmium:YAG laser ablation for the management of lower urinary tract foreign bodies following incontinence surgery: a case series and systematic review. J Endourol 30:1252–1261

Chaturvedi A, Joshi M, Mondal P, Sinha A, Srivastava A (2017) Growth of anatase and rutile phase TiO2 nanoparticles using pulsed laser ablation in liquid: influence of surfactant addition and ablation time variation. Appl Surf Sci 396:303–309

Chewchinda P, Tsuge T, Funakubo H, Odawara O, Wada H (2013) Laser wavelength effect on size and morphology of silicon nanoparticles prepared by laser ablation in liquid Japanese. J Appl Phys 52:025001

Chewchinda P et al (2014a) Preparation of Si nanoparticles by laser ablation in liquid and their application as photovoltaic material in quantum dot sensitized solar cell. In: Journal of Physics: Conference Series, vol 1. IOP Publishing, p 012023

Chewchinda P, Odawara O, Wada H (2014b) The effect of energy density on yield of silicon nanoparticles prepared by pulsed laser ablation in liquid. Appl Phys A 117:131–135

Chu L et al (2010) The improved method to determine the nucleation region of Si nanoparticles formed during pulsed laser ablation. In: 5th International Symposium on Advanced Optical Manufacturing and Testing Technologies. International Society for Optics and Photonics, pp 76553C-76553C-76555

Cleveland D, Michel RG (2008) A review of near-field laser ablation for high-resolution nanoscale surface analysis. Appl Spectrosc Rev 43:93–110

Cocherie A, Robert M (2008) Laser ablation coupled with ICP-MS applied to U–Pb zircon geochronology: a review of recent advances. Gondwana Res 14:597–608

D'Andrea C, Neri F, Ossi P, Santo N, Trusso S (2009) The controlled pulsed laser deposition of Ag nanoparticle arrays for surface enhanced Raman scattering. Nanotechnology 20: 245606

Dadashi S, Delavari H, Poursalehi R (2015) Optical properties and colloidal stability mechanism of bismuth nanoparticles prepared by Q-switched Nd:Yag laser ablation in liquid. Procedia Mater Sci 11:679–683

De Giacomo A, Gaudiuso R, Koral C, Dell'Aglio M, De Pascale O (2014) Nanoparticle enhanced laser induced breakdown spectroscopy: effect of nanoparticles deposited on sample surface on laser ablation and plasma emission. Spectrochim Acta B Atom Spectrosc 98:19–27

Desarkar H, Kumbhakar P, Mitra A (2012a) Effect of ablation time and laser fluence on the optical properties of copper nano colloids prepared by laser ablation technique. Appl Nanosci 2:285–291

Desarkar HS, Kumbhakar P, Mitra A (2012b) Optical properties of tin oxide nanoparticles prepared by laser ablation in water: influence of laser ablation time duration and laser fluence. Mater Charact 73:158–165

Dewalle P, Vendel J, Weulersse J-M, Hervé P, Decobert G (2011) Influence of carrier gas flow rate, laser repetition rate, and fluence on the size distribution and number of nanoparticles generated per laser shot during paint laser ablation. Aerosol Sci Technol 45:1429–1440

Díaz-Núñez P et al (2017) Effect of organic stabilizers on silver nanoparticles fabricated by femtosecond pulsed laser ablation. Appl Sci 7:793

Dill HG, Gerdes A, Weber B (2011) Dating of Pleistocene uranyl phosphates in the supergene alteration zone of Late Variscan granites by laser-ablation-inductive-coupled-plasma mass spectrometry with a review of U minerals of geochronological relevance to Quaternary geology. Chemie der Erde-Geochemistry 71:201–206

Dorranian D, Afshar SAA, Tahmasebi N, Eskandari AF (2014) Effect of laser pulse energy on the characteristics of Cu nanoparticles produced by laser ablation method in acetone. J Cluster Sci 25:1147–1156

Elsayed KA, Imam H, Ahmed M, Ramadan R (2013) Effect of focusing conditions and laser parameters on the fabrication of gold nanoparticles via laser ablation in liquid. Opt Laser Technol 45:495–502

Faraday M (1857) X. The Bakerian Lecture.—Experimental relations of gold (and other metals) to light. Philos Trans R Soc Lond 147:145–181

Feynman RP (2012) There's plenty of room at the bottom: an invitation to enter a new field of physics. In: Handbook of nanoscience, engineering, and technology, 3rd edn. CRC Press, pp 26–35

Gaertner G, Lydtin H (1994) Review of ultrafine particle generation by laser ablation from solid targets in gas flows. Nanostruct Mater 4:559–568

Giorgetti E, Miranda MM, Caporali S, Canton P, Marsili P, Vergari C, Giammanco F (2015a) TiO2 nanoparticles obtained by laser ablation in water: influence of pulse energy and duration on the crystalline phase. J Alloys Compd 643:S75–S79

Giorgetti E, Miranda MM, Caporali S, Canton P, Marsili P, Vergari C, Giammanco F (2015b) TiO2 nanoparticles obtained by laser ablation in water: influence of pulse energy and duration on the crystalline phase. J Alloys Compd 643:S75–S79

Gondal M, Qahtan TF, Dastageer MA, Saleh TA, Maganda YW, Anjum D (2013) Effects of oxidizing medium on the composition, morphology and optical properties of copper oxide nanoparticles produced by pulsed laser ablation. Appl Surf Sci 286:149–155

Gonzalez JJ (2017) Laser ablation–based chemical analysis techniques: a short review

Hamoudi Z, El Khakani MA, Mohamedi M (2012) Influence of pressure on the structural and electrocatalytic properties of Pt nanoparticles grown by pulsed laser ablation onto carbon paper substrate. Int J Electrochem Sci 7:1666–1676

Haram N, Ahmad N (2013) Effect of laser fluence on the size of copper oxide nanoparticles produced by the ablation of Cu target in double distilled water. Appl Phys A 111:1131–1137

Hidayah A, Triyono D, Herbani Y, Suliyanti M (2018) Effect of ablation time on femtosecond laser synthesis of Au-Ag colloidal nanoalloys. In: Journal of Physics: Conference Series, vol 1. IOP Publishing, p 012008

Hirasawa M, Orii T, Seto T (2004) Effect of insitu annealing on physical properties of Si nanoparticles synthesized by pulsed laser ablation. Appl Phys A 79:1421–1424

Hu X et al (2011) Influences of target and liquid media on morphologies and optical properties of ZnO nanoparticles prepared by laser ablation in solution. J Am Ceram Soc 94: 4305–4309

Inada M, Nakagawa H, Umezu I, Sugimura A (2003) Effects of hydrogenation on photoluminescence of Si nanoparticles formed by pulsed laser ablation. Mater Sci Eng B 101:283–285

Ismail RA, Fadhil FA (2014) Effect of electric field on the properties of bismuth oxide nanoparticles prepared by laser ablation in water. J Mater Sci Mater Electron 25:1435–1440

Ismail RA, Mousa AM, Amin MH (2018) Effect of laser fluence on the structural, morphological and optical properties of 2H-PbI 2 nanoparticles prepared by laser ablation in ethanol. J Inorg Organomet Polym Mater 28:2365–2374

Jackson T, Palmer S (1994) Oxide superconductor and magnetic metal thin film deposition by pulsed laser ablation: a review. J Phys D Appl Phys 27:1581

Johny J, Guzman SS, Krishnan B, Martinez JAA, Avellaneda DA, Shaji S (2019) SnS2 nanoparticles by liquid phase laser ablation: effects of laser fluence, temperature and post irradiation on morphology and hydrogen evolution reaction. Appl Surf Sci 470:276–288

Kim KK, Kwon HJ, Shin SK, Song JK, Park SM (2013) Stability of uncapped gold nanoparticles produced by laser ablation in deionized water: the effect of post-irradiation. Chem Phys Lett 588:167–173

Kim J, Reddy DA, Ma R, Kim TK (2014) The influence of laser wavelength and fluence on palladium nanoparticles produced by pulsed laser ablation in deionized water. Solid State Sci 37:96–102

Kim M, Osone S, Kim T, Higashi H, Seto T (2017) Synthesis of nanoparticles by laser ablation: a review. KONA Powder Part J 34:80–90

Kobayashi H, Chewchinda P, Ohtani H, Odawara O, Wada H Effects of laser energy density on silicon nanoparticles produced using laser ablation in liquid. In: Journal of Physics: Conference Series, 2013. vol 1. IOP Publishing, p 012035

Koch J, Günther D (2011) Review of the state-of-the-art of laser ablation inductively coupled plasma mass spectrometry. Appl Spectrosc 65:155A–162A

Kulinich S, Kondo T, Shimizu Y, Ito T (2013) Pressure effect on ZnO nanoparticles prepared via laser ablation in water. J Appl Phys 113:033509

Lindsay S (2010) Introduction to nanoscience. Oxford University Press

Ma Q, Saraswati TE, Ogino A, Nagatsu M (2011) Improvement of UV emission from highly crystalline ZnO nanoparticles by pulsed laser ablation under O-2/He glow discharge. Appl Phys Lett 98:051908

Maier-Komor P (1991) A review of laser ablation techniques for the preparation of vacuum deposited isotope targets. Nucl Inst Methods Phys Res B 56:921–925

Messina E (2011) Metal nanoparticles produced by pulsed laser ablation in liquid environment

Moore J, Dutta J, Tibbals H, Hornyak G (2008) Introduction to nanoscience and nanotechnology. CRC Press

Moura CG, Pereira RSF, Andritschky M, Lopes ALB, de Freitas Grilo JP, do Nascimento RM, Silva FS (2017) Effects of laser fluence and liquid media on preparation of small Ag nanoparticles by laser ablation in liquid. Opt Laser Technol 97:20–28

Muramoto J, Inmaru T, Nakata Y, Okada T, Maeda M (1999) Influence of ambient gas on formation process of Si nanoparticles by laser ablation. Appl Phys A 69:S239–S241

Nath A, Laha S, Khare A (2011) Effect of focusing conditions on synthesis of titanium oxide nanoparticles via laser ablation in titanium–water interface. Appl Surf Sci 257:3118–3122

Nikov R, Nikolov A, Nedyalkov N, Atanasov P, Alexandrov M, Karashanova D (2013) Processing condition influence on the characteristics of gold nanoparticles produced by pulsed laser ablation in liquids. Appl Surf Sci 274:105–109

Orii T, Hirasawa M, Seto T (2007) Effect of in situ annealing on structure and optical properties of ZnTe nanoparticles produced by pulsed laser ablation. In: Journal of Physics: Conference Series, vol 1. IOP Publishing, p 716

Ou Q, Shinji K, Ogino A, Nagatsu M (2008) Enhanced photoluminescence of nitrogen-doped ZnO nanoparticles fabricated by Nd:YAG laser ablation. J Phys D Appl Phys 41:205104

Pasha MA, Poursalehi R, Vesaghi M, Shafiekhani A (2010) The effect of temperature on the TCVD growth of CNTs from LPG over Pd nanoparticles prepared by laser ablation. Phys B Condens Matter 405:3468–3474

Patra N et al (2016) Parametric investigations on the influence of nano-second Nd3+:YAG laser wavelength and fluence in synthesizing NiTi nano-particles using liquid assisted laser ablation technique. Appl Surf Sci 366:104–111

Phipps C, Bohn W, Lippert T, Sasoh A, Schall W, Sinko JA (2010) Review of laser ablation propulsion. In: AIP Conference Proceedings, vol 1. AIP, pp 710–722

Piriyawong V, Thongpool V, Asanithi P, Limsuwan P (2012) Effect of laser pulse energy on the formation of alumina nanoparticles synthesized by laser ablation in water. Procedia Eng 32:1107–1112

Popovic DM, Chai JS, Zekic AA, Trtica M, Stasic J, Sarvan MZ (2014) The influence of applying the additional continuous laser on the synthesis of silicon-based nanoparticles by picosecond laser ablation in liquid. Laser Phys Lett 11:116101

Ramanujan R, Rawat R (2006) Effect of deposition parameters on morphology and size of FeCo nanoparticles synthesized by pulsed laser ablation deposition Happy, SR Mohanty, P. Lee, TL Tan, SV Springham, A. Patran. Appl Surf Sci 252:2806–2816

Resano-Garcia A, Battie Y, Koch A, En Naciri A, Chaoui N (2015) Influence of the laser light absorption by the colloid on the properties of silver nanoparticles produced by laser ablation in stirred and stationary liquid. J Appl Phys 117:113103

Riabinina D, Irissou E, Le Drogoff B, Chaker M, Guay D (2010) Influence of pressure on the Pt nanoparticle growth modes during pulsed laser ablation. J Appl Phys 108:034322

Russo RE, Mao X, Liu H, Gonzalez J, Mao SS (2002) Laser ablation in analytical chemistry—a review. Talanta 57:425–451

San NO, Kurşungöz C, Tümtaş Y, Yaşa Ö, Ortaç B, Tekinay T (2014) Novel one-step synthesis of silica nanoparticles from sugarbeet bagasse by laser ablation and their effects on the growth of freshwater algae culture. Particuology 17:29–35

Sapkota D, Li Y, Musaev OR, Wrobel JM, Kruger MB (2017) Effect of electric fields on tin nanoparticles prepared by laser ablation in water. J Laser Appl 29:012002

Scaramuzza S, Agnoli S, Amendola V (2015) Metastable alloy nanoparticles, metal-oxide nanocrescents and nanoshells generated by laser ablation in liquid solution: influence of the chemical environment on structure and composition. Phys Chem Chem Phys 17:28076–28087

Scharring S et al (2011) Review on Japanese-German-US cooperation on laser-ablation propulsion. In: AIP Conference Proceeding. vol 1. AIP, pp 47-61

Schwenke A, Wagener P, Nolte S, Barcikowski S (2011) Influence of processing time on nanoparticle generation during picosecond-pulsed fundamental and second harmonic laser ablation of metals in tetrahydrofuran. Appl Phys A 104:77–82

Setia R (2005) Modeling and diagnosis of excimer laser ablation. Citeseer

Shirk M, Molian P (1998) A review of ultrashort pulsed laser ablation of materials. J Laser Appl 10:18–28

Singh A, Vihinen J, Frankberg E, Hyvärinen L, Honkanen M, Levänen E (2017a) Effect of laser power on yield of TiO2 nanoparticles synthesized by pulsed laser ablation in water. J Ceram Sci Technol 8:39–43

Singh K, Khare A, Sharma A (2017b) Effect of uniform magnetic field on laser-produced Cu plasma and the deposited particles on the target surface. Laser Part Beams 35:352–361

Sinko JE, Sasoh A (2011) Review of CO2 Laser ablation propulsion with polyoxymethylene. Int J Aerospace Innov 3

Solati E, Mashayekh M, Dorranian D (2013) Effects of laser pulse wavelength and laser fluence on the characteristics of silver nanoparticle generated by laser ablation. Appl Phys A 112: 689–694

Solati E, Vaghri E, Dorranian D (2018) Effects of wavelength and fluence on the graphene nanosheets produced by pulsed laser ablation. Appl Phys A 124:749

Soliman W, Takada N, Sasaki K (2011) Effect of water pressure on size of nanoparticles in liquid-phase laser ablation. Jpn J Appl Phys 50:108003

Starinskiy SV, Shukhov YG, Bulgakov AV (2017) Effect of nanoparticle sizes on the extinction spectrum of colloidal solutions produced by laser ablation of gold in water. Quantum Electron 47:343

Stašić J, Živković L, Trtica M (2016) Optimization of silver nanoparticles production by laser ablation in water using a 150-ps laser. J Nanopart Res 18:366

Swarnkar R, Singh S, Gopal R (2011) Effect of aging on copper nanoparticles synthesized by pulsed laser ablation in water: structural and optical characterizations. Bull Mater Sci 34: 1363–1369

Sylvestre J-P, Kabashin AV, Sacher E, Meunier M (2005) Femtosecond laser ablation of gold in water: influence of the laser-produced plasma on the nanoparticle size distribution. Appl Phys A 80:753–758

Takada N, Fujikawa A, Koshizaki N, Sasaki K (2013) Effect of ultrasonic wave on the syntheses of Au and ZnO nanoparticles by laser ablation in water. Appl Phys A 110:835–839

Tilaki R, Mahdavi S (2007) The effect of liquid environment on size and aggregation of gold nanoparticles prepared by pulsed laser ablation. J Nanoparticle Res 9:853–860

Toosi SF, Moradi S, Hatzikiriakos SG (2017) Fabrication of micro/nano patterns on polymeric substrates using laser ablation methods to control wettability behaviour: a critical review. Rev Adhesion Adhesives 5:55–78

Torrisi L, Torrisi A (2018) Laser ablation parameters influencing gold nanoparticle synthesis in water Radiation Effects and Defects in Solids 173:729-739

Tsai M-H, Chen S-Y, Shen R-P, Shen P (2006) Laser ablation condensation of polymorphic ZrO2 nanoparticles: effects of laser parameters, residual stress, and kinetic phase change. J Appl Phys 99:054302

Tsuji T, Okazaki Y, Tsuji M (2008) Photo-induced morphological conversions of silver nanoparticles prepared using laser ablation in water—enhanced morphological conversions using halogen etching. J Photochem Photobiol A Chem 194:247–253

Tsuji M, Seto T, Otani Y (2012a) Effect of surrounding gas temperature on the morphological evolution of TiO2 nanoparticles generated by laser ablation in tubular furnace. J Nanoparticle Res 14:1–10

Tsuji T, Nakanishi M, Mizuki T, Ozono S, Tsuji M, Tsuboi Y (2012b) Preparation and shape-modification of silver colloids by laser ablation in liquids: a brief review. Sci Adv Mater 4: 391–400

Valverde-Alva M et al (2016) Laser ablation efficiency during the production of Ag nanoparticles in ethanol at a low pulse repetition rate (1–10 Hz). Laser Phys Lett 13:106002

Wang K (2013) Laser based fabrication of graphene advances in graphene. Science 2013:77–95

Wang Y-L, Xu W, Zhou Y, Chu L-Z, Fu G-S (2007a) Influence of pulse repetition rate on the average size of silicon nanoparticles deposited by laser ablation. Laser Part Beams 25:9–13

Wang Y, Xu W, Zhou Y, Chu L, Hou Y, Fu G (2007b) Influence of laser beam on transport dynamics of Si nanoparticles by laser ablation. In: 3rd International Symposium on Advanced Optical Manufacturing and Testing Technologies: Advanced Optical Manufacturing Technologies. International Society for Optics and Photonics, pp 67222H-67222H-67227

Wang Z, Zeng X, Ji M, Liu Y (2009) The effect of target size on α-Fe nanoparticle preparation by pulsed laser ablation. Appl Phys A 97:683–688

Yang G (2007) Laser ablation in liquids: applications in the synthesis of nanocrystals. Prog Mater Sci 52:648–698

Yang L, May PW, Yin L, Smith JA, Rosser KN (2007) Growth of diamond nanocrystals by pulsed laser ablation of graphite in liquid. Diamond Relat Mater 16:725–729. https://doi.org/10.1016/j.diamond.2006.11.010

Zamiranvari A, Solati E, Dorranian D (2017) Effect of CTAB concentration on the properties of graphene nanosheet produced by laser ablation. Opt Laser Technol 97:209–218

Zamora-Romero N, Camacho-Lopez MA, Camacho-Lopez M, Vilchis-Nestor AR, Castrejon-Sanchez VH, Camacho-Lopez S, Aguilar G (2019) Molybdenum nanoparticles generation by pulsed laser ablation and effects of oxidation due to aging. J Alloys Compd 788:666–671

Zhao Q, Tian G, Chen F, Zhong L, Jiang TA (2017) CT-guided percutaneous laser ablation of metastatic lung cancer: three cases report and literature review. Oncotarget 8:2187